International Journal of Pharmaceutics 669 (2025) 125108

Contents lists available at ScienceDirect

International Journal of Pharmaceutics

journal homepage: www.elsevier.com/locate/ijpharm

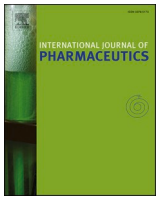

Redox/NIR dual-responsive glutathione extended polyurethane urea electrospun membranes for synergistic chemo-photothermal therapy

Annalisa Martorana [a,h,1], Giorgia Puleo [b,c,1], Giovanni Carlo Miceli [a,i], Francesco Cancilla [a], Mariano Licciardi [a], Giovanna Pitarresi [a], Luigi Tranchina [d], Maurizio Marrale [e,f], Fabio Salvatore Palumbo [a,g,*]

[a] Department of Biological, Chemical, and Pharmaceutical Sciences and Technologies (STEBICEF), University of Palermo, Via Archirafi 32, Palermo, Italy
[b] Department of Biological, Chemical and Pharmaceutical Sciences and Technologies (STEBICEF), University of Palermo, Viale delle Scienze, Edificio 18, Palermo, Italy
[c] Department of Pharmacy, University of Copenhagen, Universitetsparken 2, Copenhagen, 2100, Denmark
[d] Advanced Technologies Network (ATeN) Center, University of Palermo, Viale delle Scienze, edificio 18a, Palermo, 90128, Italy
[e] Department of Physics and Chemistry "Emilio Segrè", University of Palermo, Viale delle Scienze, edificio 18, Palermo, 90128, Italy
[f] National Institute for Nuclear Physics (INFN), Catania Division, Via Santa Sofia,64, Catania, 95123, Italy
[g] Istituto per la Ricerca e Innovazione Biomedica (IRIB), CNR, Via Ugo La Malfa, 153, 90146, Palermo, Italy
[h] Fondazione Ri.MED, c/o IRCCS ISMETT, via E. Tricomi 5, 90127, Palermo, Italy[2]
[i] Department of Bioengineering, Imperial College London, London, SW7 2BX, UK[2]

ARTICLE INFO

Keywords:
Polyurethane
Electrospinning
Gold nanorods
Photothermal therapy
Loco-regional therapy

ABSTRACT

Despite advancements in cancer treatments, therapies frequently exhibit high cytotoxicity, and surgery remains the predominant method for treating most solid tumors, often with limited success in preventing post-surgical recurrence. Implantable biomaterials, designed to release drugs at a localised site in response to specific stimuli, represent a promising approach for enhancing tumour therapy. In this study, a redox-responsive glutathione extended polyurethane urea (PolyCEGS) was used to produce paclitaxel (PTX) and gold nanorods (AuNRs) loaded electrospun membranes for combined redox/near-infrared (NIR) light-responsive release chemotherapy and hyperthermic effect. Electrospinning conditions were optimized to fabricate AuNR-loaded scaffolds, at three different AuNRs concentrations. The obtained membranes were characterized by scanning electron microscopy (SEM) analyses and photothermal profiles were evaluated by a thermocamera, showing a temperature increase, up to 42.5 °C, when exposed to NIR light (810 nm) at 3 W/cm^2. The AuNRs/PTX loaded scaffolds exhibited sustained PTX release, with 15 % released over 30 days and almost 1.8 times more in a simulated reductive environment. Moreover, their excellent photothermal effects and NIR light-triggered release led to significant synergic cytotoxicity in human colon cancer (HCT-116) and human breast cancer (MCF-7) cell lines. This system potentially enables controllable locoregional PTX release at the tumour site post-surgery, preventing recurrence and enhancing cytotoxicity through combined drug and PTT effects, highlighting its potential for future anti-cancer treatments.

1. Introduction

Post-surgical loco-regional implantation of smart biomaterials to sustain and control the release of chemotherapeutics in response to external or micro-environmental specific stimuli, is a promising strategy to reduce the risk of recurrence and achieve satisfactory outcomes while overcoming the side effects (Padmakumar and Amiji, 2023; Panthi et al., 2024; Qian et al., 2023; Shaha et al., 2024; Talebian et al., 2018; Wolinsky et al., 2012; Woodring et al., 2023). Usually, in postoperative therapy, implants such as wafers, foams, films, hydrogels, and scaffolds are employed (Aquib et al., 2020; Wolinsky et al., 2012; Zhang and Jiang, 2021). However, such systems often lack the capability for

* Corresponding author at: Department of Biological, Chemical, and Pharmaceutical Sciences and Technologies (STEBICEF), University of Palermo, Via Archirafi 32, Palermo, Italy.
E-mail address: fabiosalvatore.palumbo@unipa.it (F.S. Palumbo).
[1] Co-first authors, authors contribute equally to this manuscript.
[2] Present Addresses.

https://doi.org/10.1016/j.ijpharm.2024.125108
Received 9 October 2024; Received in revised form 18 December 2024; Accepted 18 December 2024
Available online 19 December 2024

precise, stimuli-responsive control over drug release in situ, which is critical for enhancing treatment specificity and minimizing systemic toxicity (Khan et al., 2022; Mazidi et al., 2022; Wang et al., 2022). Optimizing the drug release profiles is a key factor in developing delivery platforms in cancer therapy and, in this context, electrospinning, a straightforward method to produce drug-loaded scaffolds, can be used for these purposes (Bagó et al., 2016; Chaturvedi et al., 2024; Chen et al., 2018; Hu et al., 2014; Kuang et al., 2024; Liu et al., 2012). Over other kinds of delivery chemotherapeutics platforms, electrospun materials offer unique advantages, such as higher surface area-to-volume ratios, enhanced mechanical strength, better structural flexibility, and the capability to encapsulate the drug within the matrix making them ideal for applications requiring controlled drug delivery (Aminu et al., 2023; Ding et al., 2019a; Ramachandran et al., 2017). Programmable delivery systems with further control in modulating drug release through external and internal stimuli, can offer an even more precise approach (Dong et al., 2024; El-Husseiny et al., 2022; Kim et al., 2022; Singh et al., 2023; Tayebi-Khorrami et al., 2024; Wells et al., 2019; Xiao et al., 2023; Zhang et al., 2022). Among these stimuli, light-sensitive materials with near-infrared (NIR) photothermal properties are expected to overcome cancer recurrence through photothermal (PTT) cytotoxic effect and on-demand enhanced chemotherapic delivery triggered by localised temperature increase (Bai et al., 2019; Chen et al., 2021; Luo et al., 2019; Qu et al., 2015; Yu et al., 2019; Zhao et al., 2023). Near-infrared (NIR) light is widely used in cancer treatment due to its deep tissue penetration and low risk of damage to healthy tissues, as biological tissues are transparent to it (Chien et al., 2019; Hu et al., 2018; Zou et al., 2016). NIR light-responsive materials can be fabricated by incorporating photosensitive components, with intense absorptions in the NIR range, such as gold nanorods (AuNRs), which can generate a local temperature increase (Dunne et al., 2020; Talebian et al., 2018; Tran et al., 2015). In a localized approach, hyperthermia can be combined with chemotherapy to produce a synergistic effect. This is attributed to the increased drug release and/or the direct impact of temperature effects on the viability of cancer cells (Dunne et al., 2020; Giammona et al., 2022; Karthikeyan and Vivek, 2022; Tiwari et al., 2018; Tran et al., 2015; Wei et al., 2020; Zhang et al., 2023b). When exposed to high temperatures (up to 45 °C), cancer cells undergo apoptosis (Hervault and Thanh, 2014; Melamed et al., 2015) due to a combination of events with a large number of cellular macromolecular changes (Roti, 2008), allowing the combination of hyperthermia-chemotherapy to reduce the required dosage of anticancer drugs and improve overall therapeutic effects (Wang et al., 2017). A precise triggered release of the loaded drug can be also obtained by exploiting internal stimuli, adding another level of control in the design of the smart implant, for better localisation and increased release rate (Ding et al., 2019b; Liu et al., 2016; Ribeiro et al., 2022; Rybak et al., 2023). Redox-responsive biomaterials releasing anticancer drugs in a reductive environment can target residual cancer cells and prevent tumour recurrence, improving treatment efficacy and minimising side effects (Guo et al., 2018; Javanmardi et al., 2020; Tian et al., 2019). Indeed, after tumour resection surgery, the body's redox environment shifts due to tissue damage and healing processes (Salehi et al., 2021). Initially, oxidative stress increases, followed by a shift to a more reductive environment. However, achieving effective integration of multi-stimuli responses that can operate efficiently under physiological conditions remains challenging (Alavi et al., 2024). This highlights the need for materials that can seamlessly combine both NIR photothermal response and redox responsiveness, ensuring sustained and localized drug delivery. To integrate NIR and tissue-specific reductive responsiveness, we processed a glutathione-extended polyurethane urea derivative (PolyCEGS) into an electrospun membrane loaded with AuNRs. Indeed, the electrospinning fabrication process facilitates the simultaneous incorporation of high quantities of chemotherapeutic drugs and photothermal agents into a polymeric matrix (Cheng et al., 2014; Kaplan et al., 2016; Yang et al., 2015; Zhao and Cui, 2020). Our approach offers an advantage in addressing the limitations associated with conventional delivery systems by providing a tunable, multi-responsive platform. The combination of NIR-triggered and redox-specific drug release of the AuNRs-loaded PolyCEGS electrospun membrane demonstrated excellent PTT effects and prolonged paclitaxel release ensures a highly targeted approach.

This led to significant cytotoxic effects by using a 3D in vitro model, in two tested cancer cell lines such as human colon cancer (HCT-116) and human breast cancer (MCF-7). The results showed on-demand enhanced cytotoxicity when combining the drug with PTT, highlighting the potential of this multi-responsive drug delivery system for future anticancer treatments.

2. Materials and methods

2.1. Materials

Poly(ethylene glycol) (PEG Mw 1000 Da, labelled as PEG1K), ε −caprolactone (ε-CL), oxidized L-glutathione (GSSG), reduced L-glutathione (GSH), 5,5-dithiobis-2-nitrobenzoic acid (DTNB), ethylenediaminetetraacetic acid (EDTA), lithium bromide (LiBr), hexane, acetonitrile (ACN), diethylamine (DEA), sodium azide (NaN_3), polystyrene standards, DL-Dithiothreitol, Dulbecco's phosphate buffered saline (DPBS), BRAND® inserts, were acquired from Sigma-Aldrich Italia S.R.L. Calcium hydride (CaH_2), stannous octoate, chlorotrimethylsilane, 1,4-diisocyanatobutane (BDI), 1,1,1,3,3,3-hexafluoroisopropanol (HFIP) and trifluoroacetic acid (TFA) were purchased from Fluka, Italy. Sodium sulfite (Na_2SO_3, 98 %), glycine tetrachloroauric (III) acid trihydrate ($HAuCl_4{\cdot}3H_2O$), hexadecyltrimethylammonium bromide (CTAB), ascorbic acid, sodium borohydride ($NaBH_4$) and paclitaxel (PTX) were acquired from Merck (Germany). ECM Matrigel was purchased from Corning. The CellTiter 96# One Cell Proliferation Water Solution Assay (MTS) was purchased from Promega (Madison, WI, USA).

2.2. Methods

^{1}H-NMR spectra were recorded by Bruker Avance II 300 MHz. FT-IR spectra were obtained with Bruker Alpha instrument on KBr tablets. SEC analyses were performed using a multidetector SEC system equipped with a Water 600 pump (Mildford, MA), a Water 410 refractive index detector, and a linear Phenogel column from Phenomenex (5 μm particle size, 100 nm e 1 μm in pores size), using as eluent a solution of LiBr in DMF (0.025 M), with a flux of 0.8 mL/min at 50 °C. The calibration curve was determined using polystyrene standards (2–70 kDa). The electrospinning procedure was carried out using an NF103 Electrospinning apparatus (MECC, Fukoka, Japan). SEM micrographs were recorded with two different microscopes, a ProX PHENOM SEM (Alfatest, Italy) and a FEI FEG-ESEM (model QUANTAFEG 200). The SEM analysis was performed with an electron-accelerating voltage of 15 kV. Samples were prepared by cutting a piece of electrospun scaffold and placing it on a double-sided adhesive tape previously applied on a stainless-steel stub and dried under vacuum (0.1 Torr) before analysis. All the SEM analyses were carried out at 25.0 ± 0.1 °C, and the mean diameter of the nanofibers (d) ± standard deviation (SD) (mean ± SD, $n = 3$) was determined from the average value of 100 measurements using ImageJ software (Madison, WI, USA, version 1.46 v). Following the measurements, statistical analysis of the diameter distribution was performed with Origin Pro 2024 software. UV–Vis-NIR spectra were recorded using a Shimadzu UV 2401PC spectrophotometer (cuvette 1 mL, optical path 10 mm), from 200 nm to 900 nm. Hyperthermic studies were performed irradiating with a diode laser GBox 15A/B (GIGA Laser) at 810 nm and acquiring temperature data with an Infrared Camera FlirT250, with a resolution of 240 × 180 pixels, and a sensibility of 80 mK NETD/0,08 °C, in the range of temperature 0–70 °C. The release of PTX was evaluated with a HPLC Agilent Infinity 1290 apparatus, equipped with a Luna *C*-18 column (Phenomenex). The analyses were

performed at 25 °C, using a binary mobile phase acetonitrile/water (65:35 v/v %), with a flow rate of 1 mL/min and the detector DAD 1260 VL fixed at λ 227 nm and the software OpenLAB CDS ChemStation Workstation.

2.3. Synthesis and characterisation of PolyC$_{24}$E$_{1k}$GS

The synthesis of the poly(ether ester urethane)ureas derivative (PolyC$_{24}$E$_{1k}$GS) was performed, with few differences as reported elsewhere (Federico et al., 2022; Martorana et al., 2023; Palumbo et al., 2021). Briefly, PCL-PEG-PCL, labelled as PolyC$_{24}$E$_{1k}$ (where 24 is the ratio ε–caprolactone/poly ethylene glycol used for synthesis and 1 k the Mw of PEG used) was synthesized via Ring Opening polymerization (ROP). The methyl ester derivative of Glutathione oxidized (GSSG (OMe)$_4$) was synthesized according to our reported procedure (Martorana et al., 2023). The synthesis of PolyCEGS was finally performed. In particular, 400 mg of PolyC$_{24}$E$_{1k}$ were dispersed in DMF to reach the concentration of 115 % w/w adding 26.8 μL of BDI and 20 μL of di Sn(Ot)$_2$ 0.05 M (70 °C for 2 h). The flask was brought at 0 °C adding 79.4 mg di GSSG (OMe)$_4$ in 1.29 mL of DMF with 12.2 μL of DEA. After 2 h, the temperature was raised to 25 °C, and the reaction was performed for a further 20 h. The product was obtained by precipitating with cold diethyl ether, washing with isopropanol overnight, and finally drying under vacuum. The final product was characterized by FT-IR, ^{1}H-NMR, SEC, and colorimetric NTSB assay to detect the amount of glutathione inserted (Thannhauser et al., 1987).

2.4. Synthesis and characterization of gold nanorods (AuNRs) in CTAB

The synthesis was conducted as elsewhere reported, according to the seed-mediated procedure (Li Volsi et al., 2017; Scarabelli et al., 2015). In particular, seeds were produced by adding 25 μL of a HAuCl$_4$ solution 0.05 M to 4.7 mL of CTAB 0.1 M. Then, 300 μL of NaBH$_4$ solution 0.01 M were added to this solution under vigorous stirring. The growing solution was prepared by adding 500 μL of HAuCl$_4$ solution 0.05 M and 950 μL of HCl 1 M to 50 mL of CTAB solution 0.1 M, adding after 2 min under vigorous stirring 600 μL of AgNO$_3$ 0.01 M, 400 μL of ascorbic acid 0.1 M and 120 μL of gold seeds produced as described before. After these steps, the growing solution was left overnight in a water bath at 28 °C to allow nanoparticles to grow. The characterization of gold nanorods was performed by UV–Vis-NIR analysis the day after, and the dispersions were stored at room temperature.

2.5. Electrospinning procedure

2.5.1. AuNRs incorporation on PolyCEGS dispersion and fabrication of electrospun membranes

To embed AuNRs into the polymer dispersion, the CTAB stabilization shell was removed. In particular, eight aliquots of AuNRs@CTAB aqueous dispersion, (25 mL each) were centrifuged at 12000 rpm for 10 min. Subsequently, each pellet was dispersed in 2.5 mL of ultrapure water and the aliquots were combined to a final volume of 20 mL, thus obtaining a concentrated AuNRs dispersion. To ensure thorough removal of CTAB, two additional washing steps were performed. The total volume was then divided into three fractions of 3 mL, 6 mL, and 9 mL, respectively. The concentration of metallic gold (Au^0) was spectroscopically determined by measuring the absorbance of the three dispersions at 400 nm. According to Hendel et al. (Hendel et al., 2014), the absorbance value at 400 nm of gold nanoparticles dispersions is indicative of their Au^0 concentration, according to the following formula (Eq. (1):

$$\left[Au^0\right] = \frac{Abs_{400\ nm} \bullet 0.5}{1.2 \bullet 10^3} \quad (1)$$

Thus, it was determined that the dispersions contained 350 μg, 700 μg, and 1550 μg of Au^0, respectively. These three aliquots were then freeze-dried and labelled as Au350, Au700, and Au1550. To prepare the dispersions for electrospinning, 1 g of PolyC$_{24}$E$_{1k}$GS (from now labelled as PolyCEGS) was dispersed in 4 mL of HFIP. Simultaneously, AuNRs were dispersed in 1 mL of HFIP under mechanical stirring and sonicated for 30 min. The dispersions were placed in a 10 mL syringe, in the electrospinning device. Three different dispersions of PolyCEGS at 25 % w/v were obtained, labelled as P_Au350, P_Au700 e P_Au1550 respectively and finally processed, along with the PolyCEGS dispersion. Throughout the electrospinning process, rotational speed and translational movement were kept constant, for all the tested groups, at 40 rpm and 0.8 cm/s, respectively, while the humidity was controlled to remain within the range of 23 % to 27 %. A high-voltage generator was used to charge the steel capillary containing the polymer solution, applying a positive voltage of 13 kV for the PolyCEGS 25 % w/v and P_Au350 groups and 10 kV for the group with higher concentrations of AuNRs. The stainless-steel collector rod was maintained at ground voltage. The polymer solution was extruded at a flow rate ranging from 0.7 to 1.2 mL/h through a PTFE tube and a 21-gauge steel flat needle, with a 13 cm gap between the needle tip and the collector. Three different electrospun membrane were finally obtained and labelled as P_Au350, P_Au700 e P_Au1550 respectively. Scanning electron microscopy (SEM) was employed to investigate the electrospun membranes morphology by ProX PHENOM SEM with magnification 5000x and voltage 15 kV. Then a SEM image of P_Au1550 was acquired with higher resolution to reveal gold nanorods inside the fibers by using FEI FEG-ESEM with magnification 20000x and voltage 15 kV. To achieve the production of a chemotherapic-loaded electrospun membrane, 1 mL PTX solution in HFIP (10 % w/v) was mixed with 3 mL of a homogeneous dispersion of PolyCEGS (1 g), with 1550 μg of lyophilized AuNRs, to achieve a final PTX concentration of 1 % p/p relative to the amount of PolyCEGS. Electrospinning was performed under the same conditions used for bare PolyCEGS and P_Au1550 dispersions. Each scaffold was then prepared at least three times to assess the reproducibility of the process.

2.6. Photothermal profile of electrospun scaffolds doped with AuNRs

To investigate the relationship between Au^0 content and photothermal effect, circular samples of electrospun membranes P_Au350, P_Au700, and P_Au1550 (⌀ ≈ 1 cm; 10 mg), were placed on wells of a 48-well plate and soaked in 200 μL of DPBS at pH 7.4. Subsequently, samples were irradiated from 0 to 600 s with a diode laser at 810 nm at three different powers of emissions (2, 3, and 4 W/cm^2). An infrared camera was used to continuously monitor the temperature of the scaffolds, with data recorded at 30-second intervals. The resulting photothermal profile was reported as temperature as a function of irradiation time. Moreover, to assess any possible morphological changes in the electrospun membranes following photothermal exposure, SEM analysis were performed.

2.7. Cytocompatibility studies

The dried electrospun P_Au1550 samples were sterilized, by UV radiation at 254 nm for 20 min, using a 125 W UV lamp. Cell viability was studied on human dermal fibroblast cells (hDF) using MTS colorimetric assay. hDF cells were cultured in Dulbecco's Minimum Essential Medium (DMEM) enriched with 10 % v/v fetal bovine serum (FBS), 1 % v/v penicillin- streptomycin solution, 1 % v/v of glutamine solution and 0.1 % v/v of amphotericin B solution. The cells were kept in a flask containing 10 mL of culture medium and incubated at 37 °C in a humidified atmosphere containing 5 % of CO_2. After trypsinization, cells were counted and resuspended in DMEM. In particular, for the cytocompatibility assay, cells were seeded at the density of 1.5×10^4 cells per well on a 24-well plate to allow adhesion. After 24 h, P_Au1550 electrospun membranes and bare PolyCEGS (⌀ 0.5 cm, ~ 6 mg) were co-incubated with cells into a BRAND insert and subsequently the cell viability was

evaluated after 1, 3 and 7 days of incubation. In particular, at each selected time, mitochondrial activity was evaluated on not irradiated and irradiated samples (performing 360 s of irradiation using a diode laser at 810 nm at a power of 3 W/cm^2) recording the absorbance at a wavelength of 492 nm by a UV–Vis microplate reader (Eppendorf PlateReader AF2200). Cell viability was expressed as a percentage relative to cells incubated with culture medium alone, which were irradiated and untreated, serving as the negative control. AO/EtBr double staining assay was performed to distinguish alive and dead cells after 7 days. In order to mimic the contact occurring between membranes and tissue, a 3D assay was performed by encapsulating cells at a density of 100,000 cells/mL in Matrigel, putting then 100 μL of such dispersion on top of the electrospun scaffolds (PolyCEGS or P_Au1550) previously placed in BRAND inserts within a 48-well plate. Once the Matrigel gelled, approximately 1 mL of DMEM was added to cover the inserts, followed by incubation. Samples were treated with NIR for 2, 4, and 6 min. Cytocompatibility was assessed after 1 day of incubation. Additionally, a set of samples was irradiated for 2 min up to three times at 30-minute intervals, followed by a MTS assay.

2.8. PTX in vitro release study

Circular samples of electrospun P_Au1550 PTX loaded membrane (⌀ 0.5 cm, ~ 6 mg) were immersed in a vial with 3 mL of a 50:50 mixture of FBS/PBS or FBS/PBS containing 5 mM of DTT to simulate a reductive microenvironment. The media were collected every 24 h for the first four days, and then on days 7, 11, 15, 24, and 30. Release experiments on P_Au1550_PTX electrospun scaffolds (n = 3) were conducted both without NIR irradiation and with irradiation at a power of 3 W/cm^2, two hours before collecting the dispersing phase. Irradiation times were 2, 4, and 6 min respectively.

PTX in the release medium was quantified by extracting it with ethyl acetate (the volumetric ratio of FBS/PBS mixture to ethyl acetate was 1:3), followed by HPLC analysis after drying and solubilization in ACN/H_2O 65:35 v/v%. Drug loading (DLE %) and entrapment efficiency (EE %) percentages were calculated using a calibration curve of PTX in the range of 1–150 μg/mL, and quantification was performed on fully disaggregated scaffolds (n = 6) in HFIP.

$$\text{DLE}\,\% = \frac{\text{Weight of encapsulated PTX}}{\text{Weight of PolyCEGS} + \text{PTX}} \bullet 100 \quad (2)$$

$$\text{EE}\,\% = \frac{\text{Weight of encapsulated PTX}}{\text{Weight of total added PTX}} \bullet 100 \quad (3)$$

2.9. Cytotoxicity studies

In-vitro cytotoxicity studies were performed on human colorectal carcinoma (HCT-116) and breast cancer (MCF-7) cell lines cultivated in supplemented and enriched DMEM, incubated at 37 °C in a humidified atmosphere containing 5 % CO_2. After trypsinization, the cells were counted and encapsulated in Matrigel with a density of 1 M/mL. 100 μL of Matrigel loaded with cells were added on top of the electrospun P_Au1550 and P_Au1550_PTX membranes, previously inserted in a BRAND insert in a 48-well plate. Once the Matrigel had gelled on the scaffolds, approximately 1 mL of DMEM was added to fully cover the inserts in the wells and then incubated. The viability of cells growing in Matrigel was subsequently assessed after 1, 3, and 7 days of incubation, both assaying the samples without and with NIR irradiation at 3 W/cm^2 for 2 min. After 2 h, following treatment, the supernatant was discarded and replaced with MTS reagent to perform the viability assay. Cells were then incubated for 1 h, after which absorbance at 492 nm was recorded. Cell viability was expressed as a percentage relative to cells incubated with only culture medium, which were irradiated and untreated, serving as the negative control.

2.10. Statistical analysis

All results are reported with a mean value ± standard deviation and, when applicable the statistical analysis for significance was conducted with the Student's *t*-test, using the function *t*-test of Microsoft Excel, assuming the two-sample unequal variance and a two-tailed distribution; with a *p-value* < 0.05 were considered statistically significant.

3. Results and discussion

3.1. Synthesis of Poly$C_{24}E_{1k}$GS and NIR-light responsive electrospun scaffold production and characterization

The redox-responsive polyurethane-urea, named Poly$C_{24}E_{1k}$GS, was synthesized similarly to methods reported elsewhere (see Scheme S1) (Palumbo et al., 2021). Briefly, the synthesis involved using the prepolymer PCL-PEG-PCL as the soft chain, which was produced through ring-opening polymerization (ROP) starting from polyethylene glycol (PEG) (Mw 1 kDa), with a molar ratio of epsilon-caprolactone (ε-CL) to PEG set at 24. The hard chains consisted of BDI, and the extender used was the O-methyl derivative of Glutathione (GSSG). Data reported in Table S1, and ^{1}H-NMR spectra reported in Fig. S2 resume the physicochemical properties of prepolymer, and polyurethane urea synthesized. The incorporation of GSSG aimed to impart environmental redox responsiveness (Liu, 2019; Quinn et al., 2016). This strategy enables the development of polymers designed to selectively release drugs in response to fluctuations in redox conditions. As a result, these polymers offer targeted and efficient drug delivery mechanisms that align with the physiological conditions of the target tissue. The redox responsiveness of such series of derivatives has been already assayed in previous works (Federico et al., 2022; Martorana et al., 2023; Palumbo et al., 2021). Electrospun scaffolds and 3D printed scaffolds of Poly$C_{24}E_{1k}$GS (from now labelled as PolyCEGS) have been designed as biomaterials for locoregional release of chemically tethered Doxorubicin, demonstrating suitability for a pH and redox-responsive drug release. In addition to redox responsiveness, due to the PolyCEGS, incorporating gold nanoparticles within the polymer matrix imparts photothermal responsivity, creating a dual-responsive platform. The NIR stimulation can be externally controlled for precise localization. Besides, the redox responsiveness is triggered by biological changes in the target tissue and can respond to alterations in the tissue's normal physiological state. This dual-responsive behavior can synergistically improve the precision and efficiency of drug release.

Recent advancements in synergistic cancer therapy highlight the potential of a multi-responsive approach. For example, Gao et al. developed a dual drug co-delivery platform that combines chemotherapeutic and photothermal approaches for a more effective treatment (Gao et al., 2019). Their pH-responsive platform, utilizing black phosphorus nanosheets and a polydopamine coating, significantly improves targeted drug delivery and cellular uptake, further augmented under NIR laser irradiation. Similarly, An et al. reported the development of multi-stimuli-responsive nanoparticles combining a NIR photothermal agent and a chemotherapeutic compound (An et al., 2016). These nanoparticles exhibit NIR light, pH, and redox-responsive drug release, integrating photoinduced hyperthermia for synergistic anticancer efficiency thus leading to effective tumor ablation without regrowth. In this context, we propose that the dual redox and photothermal responsiveness, enabled by the presence of gold nanoparticles and the intrinsic redox properties of PolyCEGS, provides a significant advantage over the systems tested in our previous studies. Indeed, designing the biomaterial as an electrospun nonwoven membrane with an extremely high specific surface area, high porosity, and the capacity to entrap gold nanorods and chemotherapeutic reservoirs can further enhance its responsiveness. Fig. 1 reports a schematic illustration of the procedure to obtain the PTX/AuNRs-embedded electrospun scaffolds. This design allows for precise responses to near-infrared stimuli, resulting in a localized

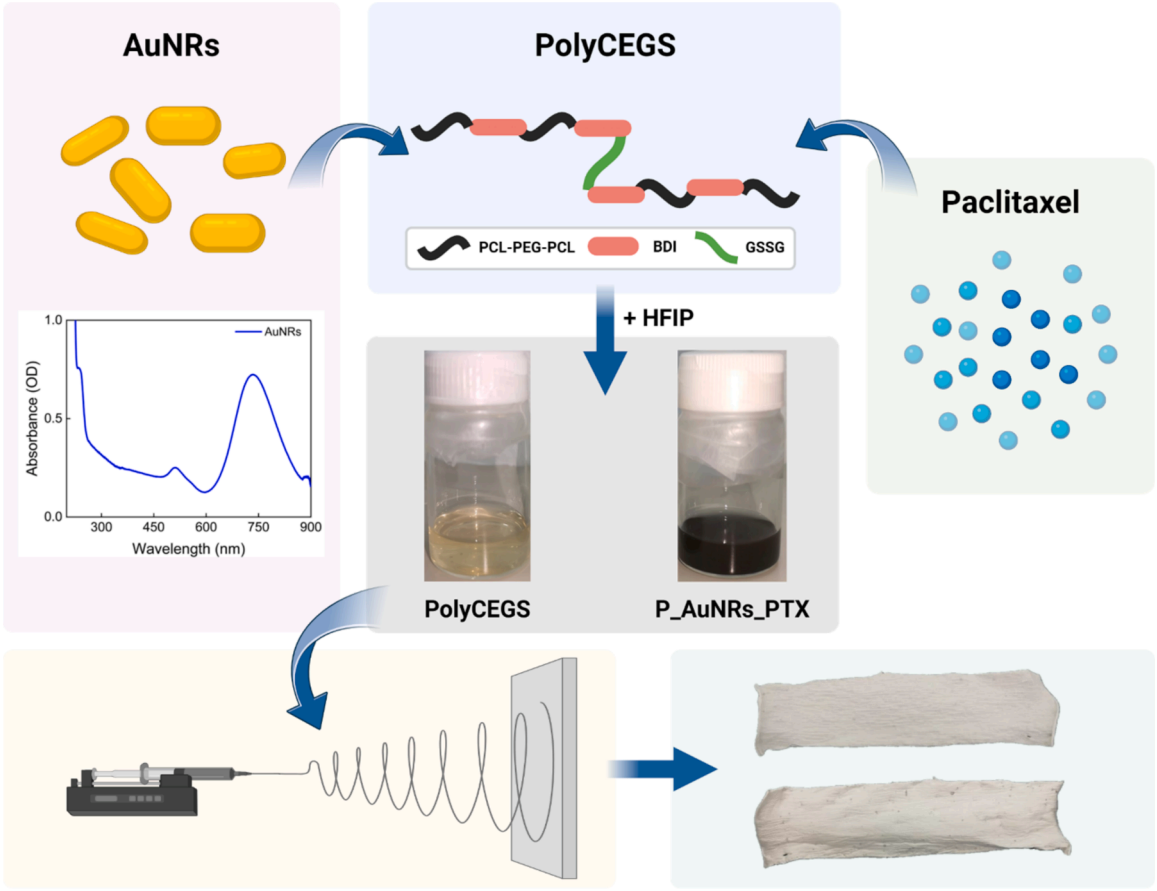

Fig. 1. Schematic illustration representing the process of preparing PolyCEGS-AuNRs-Paclitaxel electrospun scaffolds. The figure shows, from top to bottom: the three domains of PolyCEGS, the triblock copolymer PCL-PEG-PCL, BDI, and GSSG, alongside the addition of paclitaxel (PTX) and gold nanorods (AuNRs), with their UV–Vis-NIR absorption spectrum after synthesis, vials containing the HFIP-solubilized polymer dispersions (PolyCEGS and P_Au1550_PTX); and, at the bottom, the electrospinning process, with images of the front and back of the resulting electrospun scaffold representing the final product. Image created with Biorender.com.

photothermal effect and an increased rate of chemotherapeutic release (Khodadadi et al., 2020; Licciardi et al., 2022; Ma et al., 2015; Poláková et al., 2019; Zhang et al., 2014; Zhao and Cui, 2020).

First, AuNRs with consistent and desirable aspect ratios were successfully produced. We have previously demonstrated that gold nanorods with plasmonic peak lower than 810 nm effectively support photothermal activity with NIR laser irradiation (810 nm) (Li Volsi et al., 2017; Licciardi et al., 2022; Scarabelli et al., 2015; Varvarà et al., 2020). These nanorods have demonstrated limited cytotoxicity in non-tumor cell lines, and we have confirmed their efficacy in in vivo studies. Moreover, while synthesizing nanorods with a plasmonic peak closer to the laser wavelength (810 nm) might theoretically enhance their efficacy, it would require higher aspect ratios, potentially altering their shape and increasing cytotoxicity (Nogueira et al., 2020; Qiu et al., 2010). Some studies report that increasing the aspect ratio may likely lead to heightened cytotoxicity. UV–Vis analysis of the aqueous dispersions of AuNRs revealed the two characteristic plasmonic peaks, with a main peak at 748 nm (Fig. 1). This analysis allowed for the determination of the aspect ratio (R) of the nanorods, which is a critical parameter for their thermoresponsive efficiency, representing the ratio between the longitudinal and transverse axes of the nanorods.

Our results showed that the synthesized AuNRs exhibited an aspect ratio (R) of 3.44, which is within the optimal range for achieving efficient NIR responsiveness of 3 to 4, as reported by Becker et al., ensuring a significant thermal increase upon irradiation at 810 nm (Becker et al., 2010). R determination via TEM or UV–Vis analysis shows comparable results, with R correlating linearly to the peak wavelength (λ max) of the longitudinal plasmonic band, as extensively documented in the literature (Link et al., 1999).

To facilitate the dispersion of nanoparticles in the organic solvent HFIP before incorporating them with the PolyCEGS dispersion, the cationic surfactant, CTAB, was removed through multiple washing in ultrapure water. Moreover, the presence of CTAB could potentially influence the final nanocomposite properties. Additionally, the effective incorporation of nanoparticles into the polymer matrix may have been facilitated by the polymer's chemical functionalities, which potentially provide strong binding to freeze-dried not stabilized AuNRs, effectively replacing CTAB as a stabilizing agent for the nanoparticles. This is evidenced by the homogeneous distribution of gold nanoparticles within the polymer matrix, resulting in the characteristic purplish colour of the dispersion, as compared to the dispersion of the polymer alone (Fig. 1). Starting from stable and homogenized dispersions, specific electrospinning conditions were tailored for each sample to obtain the electrospun scaffolds (Fig. 1), considering the different concentrations of AuNRs, as outlined in Table 1.

The presence of gold nanorods significantly influenced both the process and the properties of the resulting nanofibers. Gold nanorods interact with the polymer matrix and the applied electric field, altering the electrospinning process. Their incorporation into the polymer dispersion influences the electrical conductivity of the polymeric solution affecting the stability of the Taylor cone (Bashouti et al., 2006; Dror et al., 2003). Moreover, they tend to align along the applied electric field during electrospinning, altering how the polymer solution extends from the Taylor cone and transforms into a fiber (Roskov et al., 2011). The incorporation of gold nanorods can enhance the mechanical properties of the nanofibers, such as tensile strength and elasticity, due to the

Table 1
Electrospinning conditions applied for different dispersions, including PolyCEGS, P_Au350, P_Au700, P_Au1550, and P_Au1550_PTX. Parameters include voltage (kV), flow rate (mL/h), transverse distance (mm), rotational frequency (rpm), translational speed (mm/s), and needle-to-collector distance.

Sample	Voltage (kV)	Flow Rate (mL/h)	Transverse Distance (mm)	Rotational Frequency (rpm)	Translational Speed (mm/s)	Needle-to-Collector Distance (mm)
PolyCEGS	13	1.2	30	40	8	130
P_Au350	13	0.8	70	40	8	130
P_Au700	10	0.7	70	40	8	130
P_Au1550	10	0.7	70	40	8	130
P_Au1550_PTX	10	0.7	70	40	8	130

reinforcement effect provided by the nanorods (Huang et al., 2021; Mahmoud et al., 2021; Turner et al., 2020). Additionally, the optical properties of the nanofibers are modified, enabling potential applications in sensing and photothermal therapy. The thermal stability of the nanofibers is also improved, as the gold nanorods can dissipate heat more efficiently. Overall, the presence of gold nanorods during the electrospinning process of polyurethane not only enhances the physical properties of the nanofibers but also provides them with multifunctional capabilities, expanding their applicability in advanced technological and biomedical fields. The resultant nanocomposite fibers hold significant potential for applications in biomedical fields, such as in drug delivery systems, tissue engineering scaffolds, and as components in advanced electronic devices.

SEM images of the four electrospun scaffolds are depicted in Fig. 2a, demonstrating a relatively uniform appearance. This is further supported by the dimensional distribution of the average fiber diameters shown in Fig. 2c, which remains consistent and increases slightly with higher AuNRs concentration. Nonetheless, all samples exhibit an average diameter distribution of around 600–800 nm. These findings support the efficacy of the electrospinning while incorporating AuNRs while preserving consistent fiber morphology, thus facilitating a tailored approach to scaffold design. The P_Au1550_PTX sample, which was not shown, had similar morphology and diameter distribution to the P_Au1550, indicating that PTX does not significantly affect the fiber morphology. Fig. 2b shows an SEM image of the P_Au1550 scaffold, captured at higher magnification and resolution to visualise the distribution of AuNRs along the nanofibers. The image suggests that the AuNRs evenly align along the fibers, likely forming clusters, which appear embedded within the polymer matrix. Defining the alignment and incorporation of AuNRs is crucial for ensuring their stable integration within the polymer matrix.

3.2. *Evaluation of the photothermal profile of electrospun scaffolds*

Several tests of the required irradiation power were conducted to determine the electrospun membrane with the best photothermal performance. For further details, please refer to the Supplementary information section. The scaffolds demonstrated temperature increases compared to bare PolyCEGS, confirming the effective incorporation of AuNRs and their photothermal stability within the polymer matrix. The sample with the lowest gold content, P_Au350, showed modest thermal behavior, reaching a maximum temperature increase of 37 °C after prolonged irradiation (>390 s). Meanwhile, samples P_Au700 and P_Au1550, with higher gold content, exhibited faster heating rates. For a comprehensive analysis, photothermal studies were also conducted on the scaffolds with lower AuNRs concentrations and at various laser powers, with these additional data provided in the Supplementary materials (see Fig. S3). Considering its superior photothermal properties,

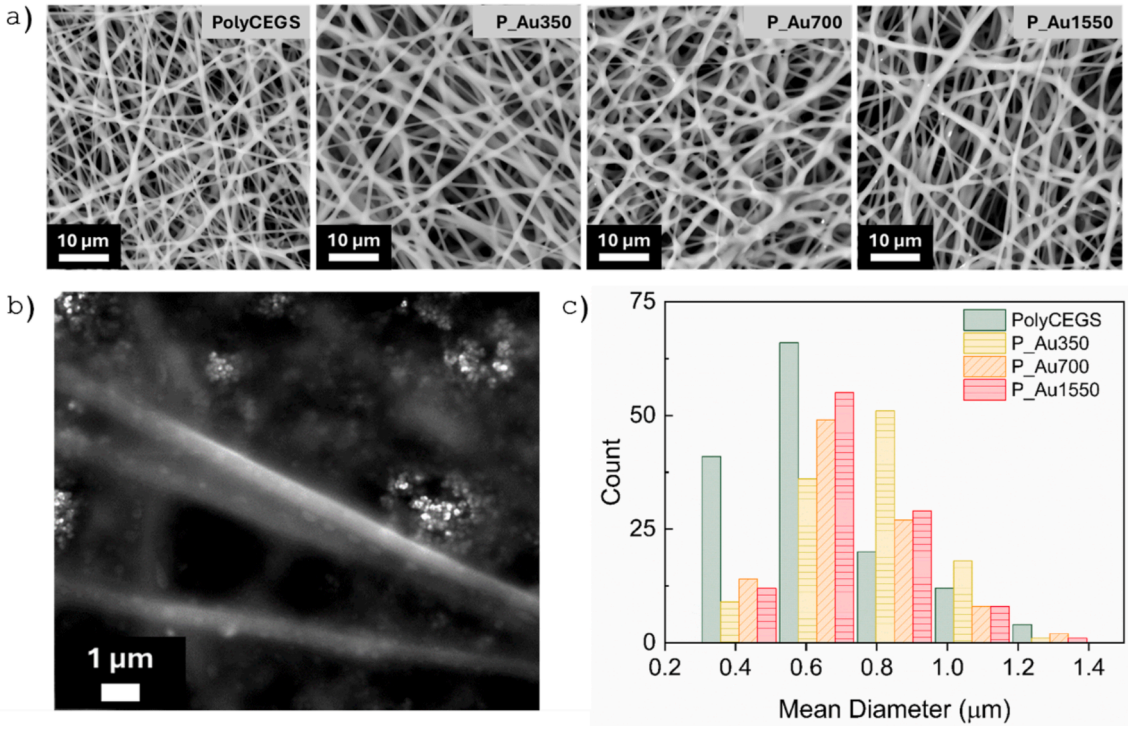

Fig. 2. Scanning electron microscopy (SEM) images of the four electrospun PolyCEGS-based scaffolds, PolyCEGS, P_Au350, P_Au700, P_Au1550. Scale bar: 10 µm, magnification: 5000x, voltage: 15 kV (a). SEM image of P_Au1550, with higher resolution to reveal gold nanorods inside the fibers. Scale bar: 1 µm, magnification: 20000x, voltage: 15 kV (b). Graph displaying the distribution of mean fiber diameters for the four scaffold types (c).

which allow it to reach the minimum required temperature for effective photothermal ablation of 42.5 °C, the P_Au1550 membranes were selected for further experimentation.

Fig. 3a illustrates the temperature profile upon irradiation at laser powers of 2, 3, and 4 W/cm^2, demonstrating a clear correlation between laser power and temperature rising. At 4 W/cm^2, the temperature rapidly surpasses 45 °C within two minutes, whereas at 2 W/cm^2, it increases more slowly, reaching a plateau around 40 °C after four minutes of irradiation. The most effective power appears to be 3 W/cm^2, achieving a gradual temperature rise to hyperthermic levels shortly after two minutes, potentially beneficial for therapeutic approaches as it helps mitigate the risk of excessive temperature spikes, which are more likely at 4 W/cm2 and could lead to unintended damage to surrounding tissues. Fig. 3b shows thermal profiles from thermal camera images, confirming the progressive temperature increase over time for all power settings. SEM images in Fig. 3c and d depict structural changes in the P_Au1550 scaffold after 10 min of laser irradiation, showing fractures and breaks likely caused by surpassing the polymer's melting temperature near the AuNRs. Despite these disruptions, absent in the native state, the overall fibrous structure of the electrospun matrix remains stable, preserving scaffold integrity and fibrillarity. These findings emphasise the importance of carefully selecting laser power to optimise photothermal therapy effectiveness while safeguarding scaffold integrity. For effective photothermal therapy, controlled temperature range achievement is crucial (Overchuk et al., 2023; Xu et al., 2022). Temperatures above 45 °C induce hyperthermia in cancer cells, leading to cell death, but significantly exceeding this threshold can damage surrounding healthy tissues and the scaffold structure (Chu and Dupuy, 2014; Lobato et al., 2023; Roti, 2008). Therefore, a laser power setting allowing a steady, controlled increase in the therapeutic temperature range, such as 3 W/cm^2, appears optimal, ensuring effective therapy while minimizing the risk of overheating or scaffold degradation.

3.3. Cytocompatibility studies

The differences between healthy and cancerous cells, which depend on their biophysical and metabolic properties, contribute to the cell selectivity of hyperthermic therapy (Bicher et al., 1980; Hegyi et al., 2013; Huang et al., 2006). The cytocompatibility assessment on the human fibroblast cell line of the materials is shown in Fig. 4. Both the bare PolyCEGS and P_Au1550 samples, demonstrate a high cytocompatibility, as evidenced by the viability of the cells growing in the well where the scaffolds were co-incubated after 1, 3, and up to 7 days and after 1 day of exposure on cells growing in Matrigel which was layered in direct contact with membranes (3D cytocompatibility assay). This observation suggests that these materials are well-tolerated by the cellular environment. Cellular viability was also assessed following laser treatment on membranes containing AuNRs, as they could cause collateral damage to the cells due to localized temperature increases. As shown in Fig. 4a, cells growing on 2D substrates co-incubated with electrospun membrane tolerated the local temperature increases. Cellular viability remained above 80 % for up to 7 days when irradiation (3 W/cm^2) was performed for 2, 4, and 6 min. This was confirmed by fluorescent images, which showed only a few dead cells when scaffolds were irradiated with a laser for 2 min. However, in 3D viability studies with cells embedded within Matrigel layered on electrospun membranes, we observed reduced viability after 6 min of NIR irradiation, indicating that prolonged, direct exposure to elevated temperatures can drastically decrease cellular functions (Fig. 4b). Conversely, the exposition of cells to cycles of 2 min of laser treatment every 30 min did not affect cell viability (Fig. 4c). The evidence indicates that laser treatment cycles, even when administered closely in time, do not have a significant cytotoxic effect.

3.4. PTX release and cytotoxicity studies

Paclitaxel (PTX), a highly effective chemotherapeutic drug, widely

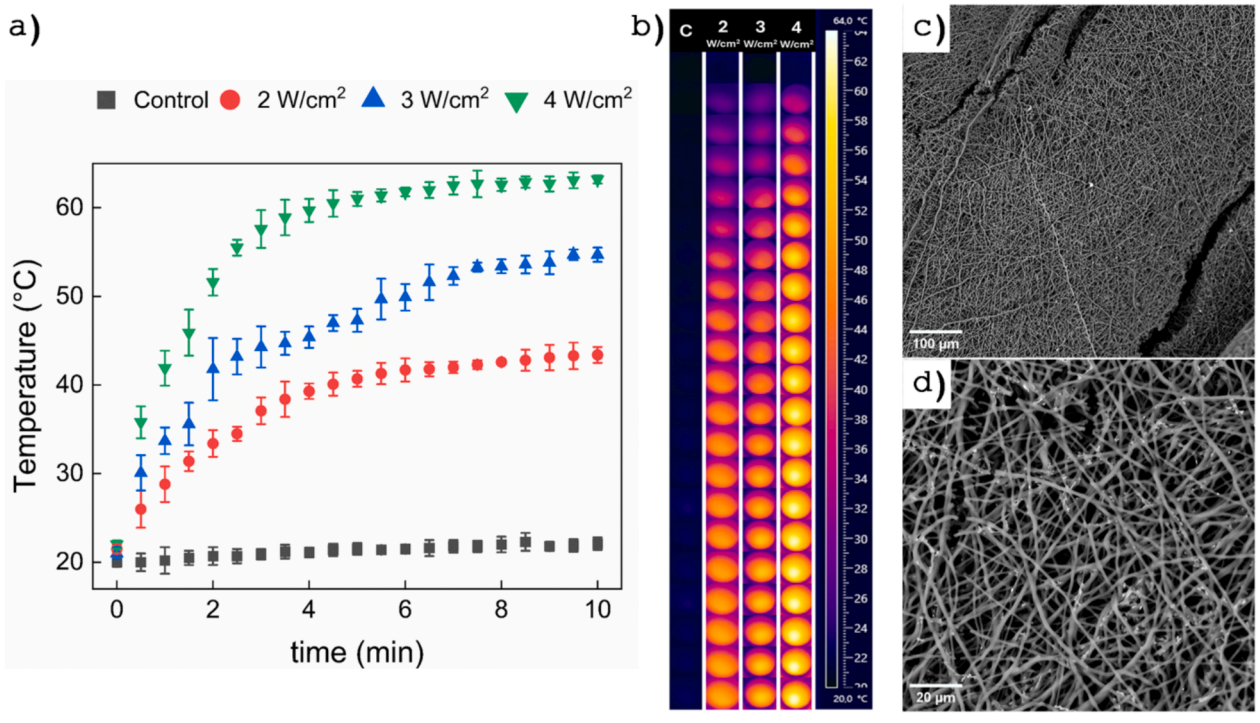

Fig. 3. Temperature-time curve showing the temperature trend during NIR laser irradiation (810 nm) at various laser powers: 2, 3, and 4 W/cm^2. The temperature of the PolyCEGS scaffold without AuNRs, serving as a control, is also displayed at 4 W/cm^2, with temperature measurements taken every 30 s for 10 min (a). NIR-thermocamera images were captured at 30-second intervals during continuous NIR irradiation at different power levels for 600 s on the P_Au1550 scaffold (b). SEM images of P_Au1550 after 10 min of NIR light irradiation at 3 W/cm^2: 400x magnification (c), 2000x magnification (d).

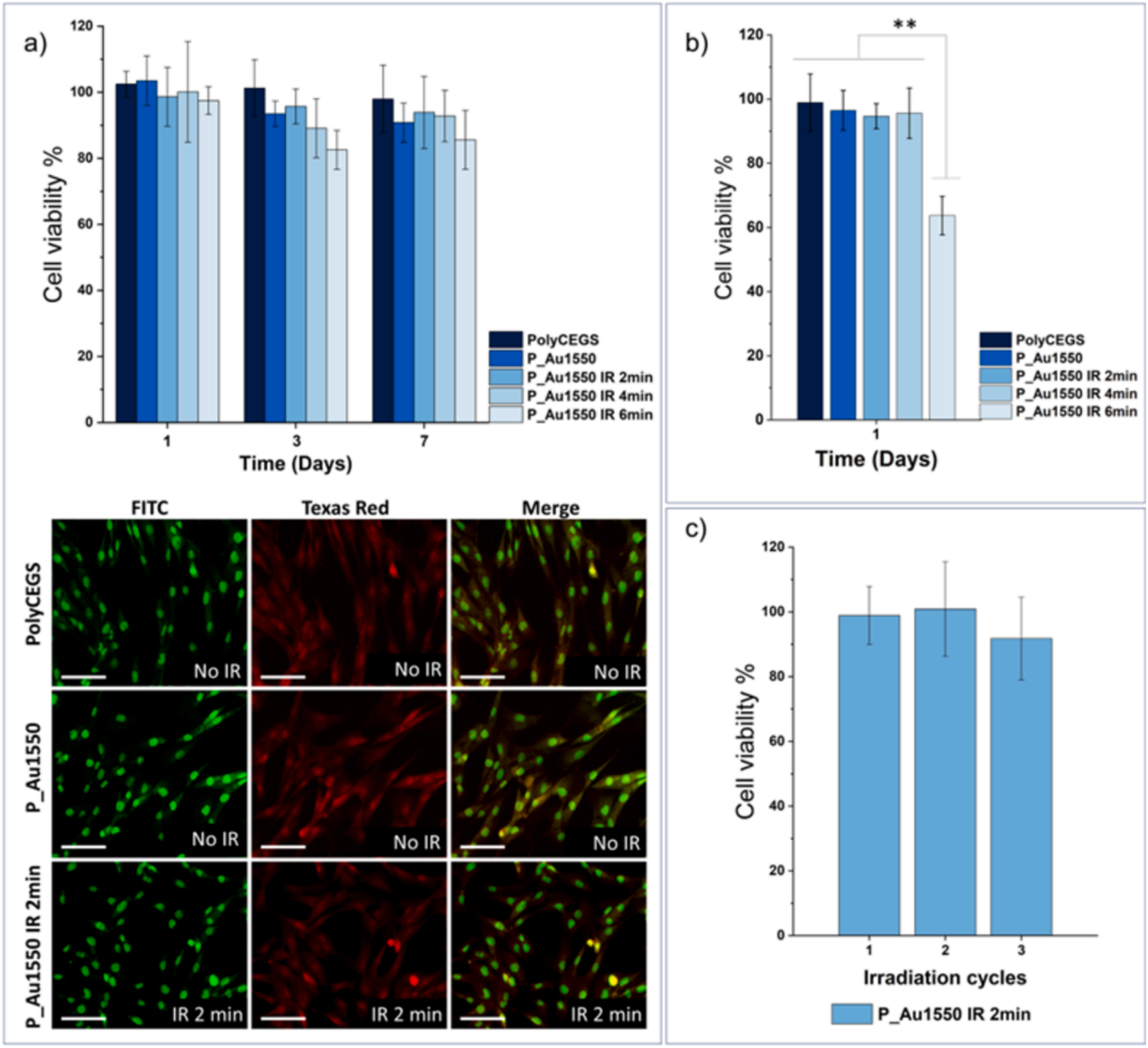

Fig. 4. Cell viability (%) of cells growing in a bi-dimensional well in the presence of the scaffolds with and without AuNRs, both untreated and treated with NIR irradiation (3 W/cm^2) for 2, 4 and 6 min after 1, 3 and 7 days of incubation; images of AO/EtBr stained fibroblasts (scale bar: 100 μm) after 7 days of incubation treated with PolyCEGS (not irradiated, No IR) and P_Au1550, either not irradiated (No IR) or irradiated (IR) for 2 min at a power of 3 W/cm^2 (a). Cell viability % of fibroblasts growing on Matrigel layered in direct contact with P_Au1550 and PolyCEGS membranes not irradiated and irradiated with NIR (3 W/cm^2) for 2, 4, and 6 min after 1 day of incubation (**$p < 0.01$) (b). Cell viability % of fibroblasts growing on Matrigel layered in direct contact with P_Au1550 and PolyCEGS membranes irradiated at 3 W/cm^2 for 2 min repeated 1, 2, and 3 times every 30 min (c).

employed in the treatment of various solid tumours (Ma and Mumper, 2013; Sharifi-Rad et al., 2021; Zhou et al., 2021), has been effectively incorporated into the electrospun membranes. This incorporation offers several potential advantages. Firstly, it allows for localized delivery of the drug to the tumour site, minimizing systemic toxicity. Secondly, the sustained release kinetics of PTX from the scaffolds can provide prolonged exposure to the therapeutic agent, potentially enhancing its efficacy. Furthermore, the combination of PTX with the photothermal activity of the scaffolds synergistically improves therapeutic outcomes by inducing tumour cell death through multiple mechanisms, including disruption of microtubule dynamics and hyperthermia-induced cytotoxicity (Azerbaijan et al., 2021; Chen et al., 2015; Ren et al., 2013; Sang et al., 2021; Su et al., 2018; Tiwari et al., 2018; You et al., 2010). Considering the results of the cytocompatibility study, two different NIR (810 nm) irradiation times (2 and 4 min) were selected to evaluate the release of PTX kinetics in response to NIR light exposure. To investigate the drug release profile, given PTX's poor solubility in aqueous solvents, the studies were conducted using a PBS/FBS mixture (v/v % = 50/50) and quantified through HPLC analysis (Abouelmagd et al., 2015).

The drug loading efficiency (DLE) of PTX was 0.96 % and the entrapment efficiency (EE) was 96.5 % ± 0.9. As shown in Fig. 5a, in phosphate buffer/FBS (1:1) after an initial rapid release of PTX due to the burst effect, not irradiated (NI) PolyCEGS electrospun membranes demonstrated a sustained release profile over time. A sharp and statistically significant increase in PTX release was triggered by NIR irradiation. No significant differences were observed during the first 2 days of analysis due to the high release rate. However, after 3 days, the amount of released drug increased by about 50 % compared to the non-irradiated sample. No statistically significant differences were observed between 2 and 4 min of irradiation.

The release rate increased significantly in a reductive environment (mimicked by the presence of DTT) (Fig. 5b), with the total amount of

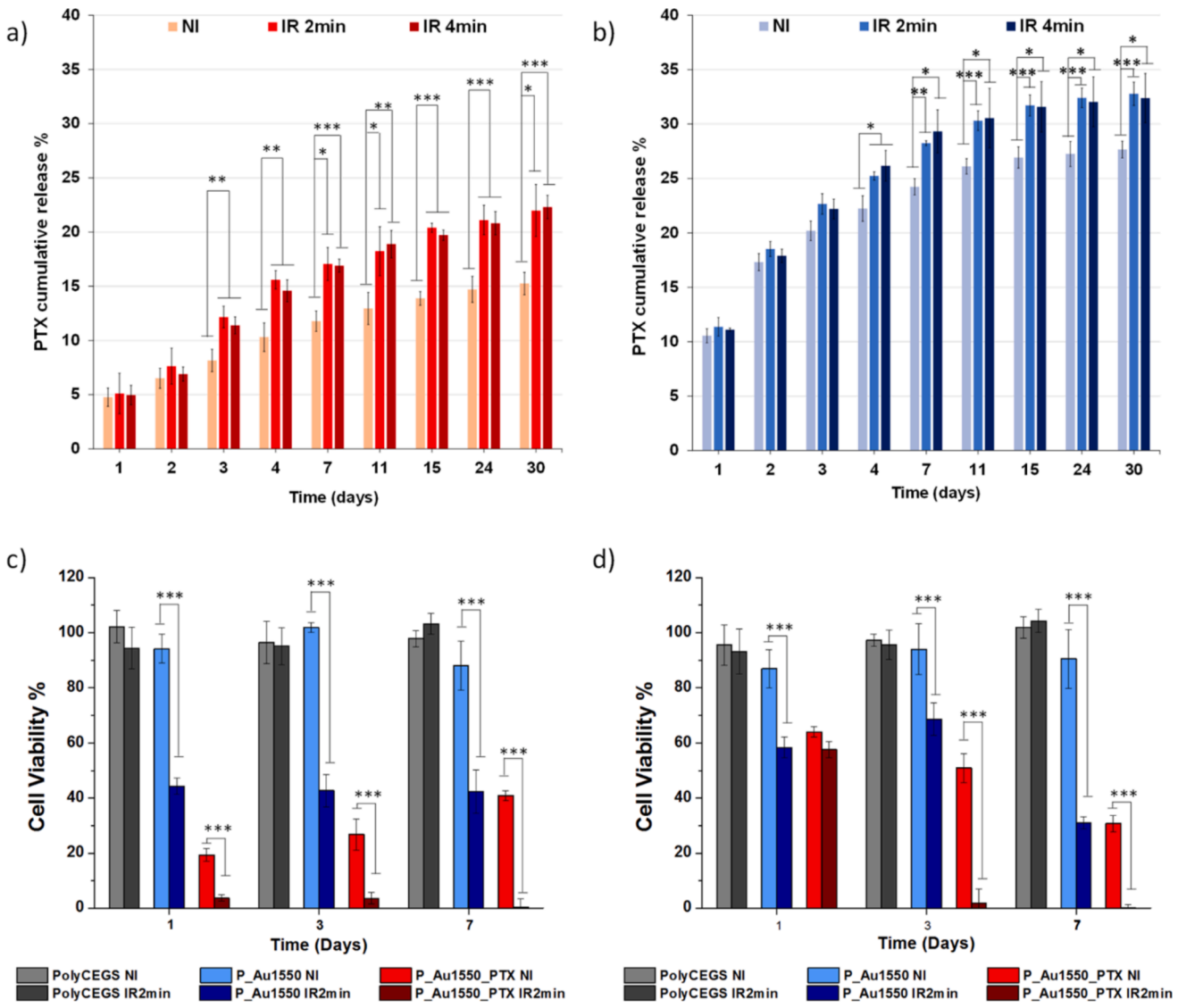

Fig. 5. Cumulative % release of PTX over time for non-irradiated (NI), and irradiated samples for 2 and 4 min in phosphate buffer/FBS (1:1) (a); 5 mM DTT phosphate buffer/FBS (1:1) (b). Cytotoxicity studies on HCT-116 (c) and MCF-7 (d) (*$p < 0.05$, **$p < 0.01$, ***$p < 0.005$).

drug released almost doubling at each time point compared to the release profile observed without DTT. This behaviour strongly confirms the sharp redox responsiveness of PolyCEGS, which is further enhanced by the direct entrapment of PTX in the fibres and the increased surface-to-volume ratio of the electrospun membrane. As expected, due to the significant stimulation of the release rate by DTT, the effect of NIR irradiation was less pronounced.

To study the cytotoxicity of electrospun scaffolds on tumor cell lines, we conducted a MTS viability assay on HCT-116 cells and MCF-7 cells. We designed a simple but effective in vitro model using Matrigel to create a 3D scaffold for tumor cell growth. This scaffold was layered on the surface of the electrospun membrane to mimic the contact between the medicated electrospun membrane and tissue during locoregional application. Compared to direct analysis of the PTX cytotoxic effect in cell-growing medium, this model better correlates the cytotoxic effect to the PTX diffusion through the Matrigel with the NIR responsive cytotoxic effect. Moreover, 3D cell culture better simulates the tumor microenvironment, including hypoxia, pH and redox state, and cell–cell interactions, crucial to study the antitumor activity of the system (Abuwatfa et al., 2024; Datta et al., 2020; Lv et al., 2017; Zhang et al., 2023a). 3D cell cultures exhibited an increase in drug resistance compared to the 2D cell culture, better showing the importance of the combination of chemotherapy with photothermal therapy (Barbosa et al., 2022; Breslin and O'Driscoll, 2016; Dong et al., 2012; Edmondson et al., 2014; Fisher and Rao, 2020; Fontoura et al., 2020; Zhao et al., 2014). In Supplementary materials (Fig. S4a), a representation of the 3D cell culture method using a Matrigel matrix is provided, which was subsequently used to assess cell viability on the scaffolds. Moreover, Fig. S4b showed HCT-116 and MCF-7 3D cell viability in Matrigel showing that no statistical differences were observed with and without NIR irradiation.

Bare PolyCEGS, P_Au1550, and P_Au1550_PTX, not subjected and subjected to NIR irradiation, were investigated after 1, 3, and 7 days of incubation. Based on drug release results and considering the need to limit normal cells' exposure to high temperatures, we selected 2 min of irradiation at 3 W/cm^2. As expected, HCT-116 cells were viable in contact with the bare PolyCEGS membrane, both without (not irradiated NI samples) and under NIR-irradiation (IR samples). Instead, the NIR-irradiated P_Au1550 membrane led to a significant decrease in HCT-116 viability which stabilized around 45 % during 1, 3, and 7 days of NIR stimulation, thus confirming the high cytoreductive potential of the photothermal effect.

The P_Au1550_PTX membrane in the NI experiment caused a sharp decrease (20 %) in HCT-116 viability after 1 day. However, this decrease

was less pronounced after 3 and 7 days showing instead a slight increase to 30 and 40 % of viability respectively. This can be attributed to the sustained slow diffusion of PTX from the electrospun membrane and the increased growth of cells in Matrigel, which showed reduced susceptibility to the released PTX (Karlsson et al., 2012).

The NIR-stimulated P_Au1550_PTX membrane demonstrated the synergism between the NIR photothermal and PTX chemotherapeutic effect resulting in a strong reduction in HCT-116 viability, reaching its maximum at 7 days with complete inhibition of cellular viability. Compared to HCT-116, MCF-7 cells showed (see Fig. 5d), reduced susceptibility to the treatment with not irradiated P_Au1550_PTX membrane, although a progressive increase in cytotoxicity was observed from 1 to 7 days. NIR irradiation on the P_Au1550_PTX membrane produced a strong cytotoxic effect after 3 and 7 days of treatment, comparable to that observed for HCT-116. We believe variations in response may be attributed primarily to the differing proliferation rates of these cell lines when cultured in Matrigel, as evidenced in Fig. S4 of the Supplementary materials. Specifically, HCT-116 cells exhibit a significantly higher metabolic activity at day 1 compared to MCF-7 cells. This characteristic may enhance the effect of PTX making its impact more pronounced in rapidly dividing HCT-116 cells (Liebmann et al., 1993). In contrast, the effect of paclitaxel on MCF-7 cells becomes more apparent after a longer incubation period. Additionally, it is known that both cell lines form clusters when embedded in 3D gels, such as Matrigel, better simulating physiological conditions, which can limit drug penetration and reduce the initial cytotoxic response, thus confirming the need of the combined effect of PTX release and the photothermal effect to improve efficiency (Ashworth et al., 2020; Cavo et al., 2016; Krause et al., 2010; Pamplona et al., 2024; Petersen et al., 1992; Yeung et al., 2010).

We already observe redox sensitivity in the drug release profile, and we can hypothesize that the high cell density and 3D culture may lead to oxygen depletion, simulating a tumor redox environment (Aggarwal et al., 2020; D'Aiuto et al., 2022; Gilkes et al., 2014; Jin et al., 2007; Sheta et al., 2001; Taddei et al., 2013). This can lead to alterations in the redox balance within the extracellular environment, which may impact the drug release mechanism and contribute to differences in cytotoxic effects between the cell lines. The hypoxic state can increase reactive oxygen species (ROS) production and glutathione (GSH) levels, resulting from oxidative stress (Ma et al., 2024; Zeng et al., 2018). GSH trigger thiol-disulfide exchange reactions, breaking the disulfide bonds to release therapeutic agents (Guo et al., 2018; Lee et al., 2013). While, in high ROS environments, disulfide bonds can undergo oxidative reactions, forming sulfone or sulfoxide, which enhance hydrophilicity. This change facilitates hydrolysis, promoting carrier disintegration and drug release (Sun et al., 2018).

4. Conclusions

This study focused on developing multi-responsive paclitaxel (PTX) and gold nanorods (AuNRs) loaded electrospun membranes, based on a redox-responsive polyurethane urea (PUU), designed to provide a localized and controlled release of chemotherapeutics in response to near-infrared (NIR) light and redox changes in the tumor microenvironment. The study successfully demonstrates the fabrication of PUU nanofibers incorporating AuNRs and PTX through optimized electrospinning conditions. The photothermal properties were validated by the controlled temperature increase upon NIR irradiation (3 W/cm^2, 810 nm), achieving effective hyperthermia (42.5 °C) after 2 min, while maintaining scaffold stability. Furthermore, the cytocompatibility of the PUU-AuNRs scaffolds ensures minimal damage to healthy tissues, enhancing their clinical relevance. Cytocompatibility studies confirmed the scaffolds' safety in a cellular environment, demonstrating over 80 % cell viability under laser treatment, highlighting their potential for non-toxic clinical applications.

The scaffold showed a sustained PTX release profile, significantly enhanced in reductive environments, mimicking post-surgical conditions. Such an environment-responsive behavior suggests an efficient mechanism for localized chemotherapy delivery, maintaining therapeutic concentrations with reduced systemic exposure. The dual-response mechanism allows for synergistic hyperthermia and chemotherapy, leading to a substantial reduction in cancer cell viability in vitro, as evidenced by experiments on human breast cancer (MCF-7) and colon cancer (HCT-116) cell lines.

In conclusion, the development of PUU-based electrospun scaffolds present a promising strategy for post-surgical cancer treatment. While this study demonstrates the potential of combining chemotherapy with photothermal therapy (PTT), several critical challenges must be addressed for clinical translation. Bridging the gap between innovative materials and clinical application requires key steps such as rigorous preclinical testing, adherence to stringent regulatory requirements, standardization in manufacturing processes, carefully designed clinical trials, and active collaboration with clinical and industrial stakeholders. The design of an electrospun material for locoregional application provides a potential solution to overcoming targeting efficiency challenges. As demonstrated in this study, our system enhances responsiveness to external stimulation and sharpens the precision of drug release at the desired site. This localized and controllable delivery approach may help overcome some barriers to clinical translation. Furthermore, preclinical in vivo testing represents a logical next step for confirming the safety, efficacy, and biocompatibility of the designed platform.

Funding sources

This research has received founding from MIUR.

Declaration of generative AI and AI-assisted technologies in the writing process

During the preparation of this work the authors used OpenAI's GPT-4 model, in order to improve text clarity and grammar checks. After using this tool/service, the authors reviewed and edited the content as needed and take full responsibility for the content of the published article.

CRediT authorship contribution statement

Annalisa Martorana: Writing – review & editing, Writing – original draft, Visualization, Validation, Methodology, Investigation, Formal analysis, Data curation, Conceptualization. **Giorgia Puleo:** Writing – review & editing, Writing – original draft, Visualization, Validation, Methodology, Investigation, Formal analysis, Data curation, Conceptualization. **Giovanni Carlo Miceli:** Writing – review & editing, Methodology, Investigation. **Francesco Cancilla:** Methodology, Investigation, Data curation. **Mariano Licciardi:** Writing – review & editing, Supervision, Project administration. **Giovanna Pitarresi:** Writing – review & editing, Supervision, Funding acquisition. **Luigi Tranchina:** Methodology. **Maurizio Marrale:** Methodology. **Fabio Salvatore Palumbo:** Conceptualization, Methodology, Project administration, Supervision, Validation, Visualization, Writing – original draft, Writing - review and editing, Funding acquisition.

Declaration of competing interest

The authors declare that they have no known competing financial interests or personal relationships that could have appeared to influence the work reported in this paper.

Acknowledgements

Authors thank Advanced Technologies Network Center (ATeN Center-Laboratory of Preparation and Analysis of Biomaterials) and Francesco Paolo Bonomo for SEM analysis.

Giorgia Puleo acknowledges the financial support from the VILLUM FONDEN by the Villum Young Investigator Grants "Protein superstructure as Smart Biomaterials (ProSmart)" 2018-2023 (project number: 19175) and "Protein Phase Separation and Solid Transition in Synthetic Cells (ProSeC) 2024-2027 (project number: 53132), and from the Novo Nordisk Foundation (projects NNF20OC0065260 and NNF22OC0080141).

Appendix A. Supplementary data

Supplementary data to this article can be found online at https://doi.org/10.1016/j.ijpharm.2024.125108.

Data availability

The authors are unable or have chosen not to specify which data has been used.

References

Abouelmagd, S.A., Sun, B., Chang, A.C., Ku, Y.J., Yeo, Y., 2015. Release kinetics study of poorly water-soluble drugs from nanoparticles: Are we doing it right? Mol. Pharm. 12, 997. https://doi.org/10.1021/mp500817h.

Abuwatfa, W.H., Pitt, W.G., Husseini, G.A., 2024. Scaffold-based 3D cell culture models in cancer research. J. Biomed. Sci. 31, 7. https://doi.org/10.1186/s12929-024-00994-y.

Aggarwal, V., Miranda, O., Johnston, P.A., Sant, S., 2020. Three dimensional engineered models to study hypoxia biology in breast cancer. Cancer Lett. 490, 124–142. https://doi.org/10.1016/j.canlet.2020.05.030.

Alavi, S.E., Alharthi, S., Alavi, S.Z., Raza, A., Ebrahimi Shahmabadi, H., 2024. Bioresponsive drug delivery systems. Drug Discov. Today 29. https://doi.org/10.1016/j.drudis.2023.103849.

Aminu, N., Ilyasu, S., Al-Kassim Hassan, M., Kurfi, F.S., Jatau, A.I., Chan, S.Y., Alfred-Ugbenbo, D., 2023. Applications of nanofibers drug delivery system in cancer therapy. J. Drug Deliv. Sci. Technol. 90, 105128. https://doi.org/10.1016/j.jddst.2023.105128.

An, X., Zhu, A., Luo, H., Ke, H., Chen, H., Zhao, Y., 2016. Rational design of multi-stimuli-responsive nanoparticles for precise cancer therapy. ACS Nano 10, 5947–5958. https://doi.org/10.1021/acsnano.6b01296.

Aquib, M., Juthi, A.Z., Farooq, M.A., Ali, M.G., Janabi, A.H.W., Bavi, S., Banerjee, P., Bhosale, R., Bavi, R., Wang, B., 2020. Advances in local and systemic drug delivery systems for post-surgical cancer treatment. J. Mater. Chem. B 8, 8507–8518. https://doi.org/10.1039/d0tb00987c.

Ashworth, J.C., Thompson, J.L., James, J.R., Slater, C.E., Pijuan-Galitó, S., Lis-Slimak, K., Holley, R.J., Meade, K.A., Thompson, A., Arkill, K.P., Tassieri, M., Wright, A.J., Farnie, G., Merry, C.L.R., 2020. Peptide gels of fully-defined composition and mechanics for probing cell-cell and cell-matrix interactions in vitro. Matrix Biol. 85–86, 15–33. https://doi.org/10.1016/j.matbio.2019.06.009.

Azerbaijan, M.H., Bahmani, E., Jouybari, M.H., Hassaniazardaryani, A., Goleij, P., Akrami, M., Irani, M., 2021. Electrospun gold nanorods/graphene oxide loaded-core-shell nanofibers for local delivery of paclitaxel against lung cancer during photo-chemotherapy method. Eur. J. Pharm. Sci. 164, 105914. https://doi.org/10.1016/j.ejps.2021.105914.

Bagó, J.R., Pegna, G.J., Okolie, O., Mohiti-Asli, M., Loboa, E.G., Hingtgen, S.D., 2016. Electrospun nanofibrous scaffolds increase the efficacy of stem cell-mediated therapy of surgically resected glioblastoma. Biomaterials 90, 116–125. https://doi.org/10.1016/j.biomaterials.2016.03.008.

Bai, G., Yuan, P., Cai, B., Qiu, X., Jin, R., Liu, S., Li, Y., Chen, X., 2019. Stimuli-responsive scaffold for breast cancer treatment combining accurate photothermal therapy and adipose tissue regeneration. Adv. Funct. Mater. 29, 1904401. https://doi.org/10.1002/adfm.201904401.

Barbosa, M.A.G., Xavier, C.P.R., Pereira, R.F., Petrikaitė, V., Vasconcelos, M.H., 2022. 3D cell culture models as recapitulators of the tumor microenvironment for the screening of anti-cancer drugs. Cancers (Basel) 14, 190. https://doi.org/10.3390/cancers14010190.

Bashouti, M., Salalha, W., Brumer, M., Zussman, E., Lifshitz, E., 2006. Alignment of Colloidal CdS Nanowires Embedded in Polymer Nanofibers by Electrospinning. Chem. Phys. Chem 7, 102–106. https://doi.org/10.1002/cphc.200500428.

Becker, J., Trügler, A., Jakab, A., Hohenester, U., Sönnichsen, C., 2010. The optimal aspect ratio of gold nanorods for plasmonic bio-sensing. Plasmonics 5. https://doi.org/10.1007/s11468-010-9130-2.

Bicher, H.I., Hetzel, F.W., Sandhu, T.S., Frinak, S., Vaupel, P., O'Hara, M.D., O'Brien, T., 1980. Effects of hyperthermia on normal and tumor microenvironment. Radiology 137, 523–530. https://doi.org/10.1148/radiology.137.2.7433686.

Breslin, S., O'Driscoll, L., 2016. The relevance of using 3D cell cultures, in addition to 2D monolayer cultures, when evaluating breast cancer drug sensitivity and resistance. Oncotarget 7, 45745. https://doi.org/10.18632/oncotarget.9935.

Cavo, M., Fato, M., Peñuela, L., Beltrame, F., Raiteri, R., Scaglione, S., 2016. Microenvironment complexity and matrix stiffness regulate breast cancer cell activity in a 3D in vitro model. Sci. Reports 6, 35367. https://doi.org/10.1038/srep35367.

Chaturvedi, S., Rastogi, V., Kumar, M., 2024. An insight on nanofibers assisted localized delivery of anti-cancer drugs to breast for an effective breast cancer treatment. J. Drug Deliv. Sci. Technol. 93, 105447. https://doi.org/10.1016/j.jddst.2024.105447.

Chen, S., Boda, S.K., Batra, S.K., Li, X., Xie, J., 2018. Emerging roles of electrospun nanofibers in cancer research. Adv. Healthc. Mater. 7, e1701024. https://doi.org/10.1002/adhm.201701024.

Chen, Q., Liang, C., Wang, C., Zhuang, L., 2015. An imagable and photothermal "Abraxane-Like" nanodrug for combination cancer therapy to treat subcutaneous and metastatic breast tumors. Adv. Mater. 27, 903–910. https://doi.org/10.1002/adma.201404308.

Chen, L., Yu, Q., Cheng, K., Topham, P.D., Xu, M., Sun, X., Pan, Y., Jia, Y., Wang, S., Wang, L., 2021. Can photothermal post-operative cancer treatment be induced by a thermal trigger? ACS Appl. Mater. Interfaces 13, 60837–60851. https://doi.org/10.1021/acsami.1c16283.

Cheng, M., Wang, H., Zhang, Z., Li, N., Fang, X., Xu, S., 2014. Gold nanorod-embedded electrospun fibrous membrane as a photothermal therapy platform. ACS Appl. Mater. Interfaces 6, 1569–1575. https://doi.org/10.1021/am405839b.

Chien, Y.H., Chan, K.K., Anderson, T., Kong, K.V., Ng, B.K., Yong, K.T., 2019. Advanced near-infrared light-responsive nanomaterials as therapeutic platforms for cancer therapy. Adv. Ther. 2, 1800090. https://doi.org/10.1002/adtp.201800090.

Chu, K.F., Dupuy, D.E., 2014. Thermal ablation of tumours: biological mechanisms and advances in therapy. Nat. Rev. Cancer 14, 199–208. https://doi.org/10.1038/nrc3672.

D'Aiuto, N., Hochmann, J., Millán, M., Di Paolo, A., Bologna-Molina, R., Sotelo Silveira, J., Arocena, M., 2022. Hypoxia, acidification and oxidative stress in cells cultured at large distances from an oxygen source. Sci. Reports 12, 21699. https://doi.org/10.1038/s41598-022-26205-y.

Datta, P., Dey, M., Ataie, Z., Unutmaz, D., Ozbolat, I.T., 2020. 3D bioprinting for reconstituting the cancer microenvironment. npj PrecisOncol. 4, 18. https://doi.org/10.1038/s41698-020-0121-2.

Ding, Y., Li, W., Zhang, F., Liu, Z., Zanjanizadeh Ezazi, N., Liu, D., Santos, H.A., 2019a. Electrospun fibrous architectures for drug delivery, tissue engineering and cancer therapy. Adv. Funct. Mater. 29, 1802852. https://doi.org/10.1002/adfm.201802852.

Ding, Y., Liu, J., Li, X., Xu, L., Li, C., Ma, L., Liu, J., Ma, R., An, Y., Huang, F., Liu, Y., Shi, L., 2019b. Rational design of drug delivery systems for potential programmable drug release and improved therapeutic effect. Mater. Chem. Front. 3, 1159–1167. https://doi.org/10.1039/c9qm00178f.

Dong, Y., Fu, S., Yu, J., Li, X., Ding, B., 2024. Emerging smart micro/nanofiber-based materials for next-generation wound dressings. Adv. Funct. Mater. 34, 2311199. https://doi.org/10.1002/adfm.202311199.

Dong, X.L., Xu, P.F., Miao, C., Fu, Z.Y., Li, Q.P., Tang, P.Y., Wang, T., 2012. Hypoxia decreased chemosensitivity of breast cancer cell line MCF-7 to paclitaxel through cyclin B1. Biomed. Pharmacother. 66, 70–75. https://doi.org/10.1016/j.biopha.2011.11.016.

Dror, Y., Salalha, W., Khalfin, R.L., Cohen, Y., Yarin, A.L., Zussman, E., 2003. Carbon nanotubes embedded in oriented polymer nanofibers by electrospinning. Langmuir 19, 7012–7020. https://doi.org/10.1021/la034234i.

Dunne, M., Regenold, M., Allen, C., 2020. Hyperthermia can alter tumor physiology and improve chemo- and radio-therapy efficacy. Adv. Drug Deliv. Rev. 163–164, 98–124. https://doi.org/10.1016/j.addr.2020.07.007.

Edmondson, R., Broglie, J.J., Adcock, A.F., Yang, L., 2014. Three-dimensional cell culture systems and their applications in drug discovery and cell-based biosensors. Assay Drug Dev. Technol. 12, 207. https://doi.org/10.1089/adt.2014.573.

El-Husseiny, H.M., Mady, E.A., Hamabe, L., Abugomaa, A., Shimada, K., Yoshida, T., Tanaka, T., Yokoi, A., Elbadawy, M., Tanaka, R., 2022. Smart/stimuli-responsive hydrogels: Cutting-edge platforms for tissue engineering and other biomedical applications. Mater. Today Bio 13, 100186. https://doi.org/10.1016/j.mtbio.2021.100186.

Federico, S., Martorana, A., Pitarresi, G., Palumbo, F.S., Fiorica, C., Giammona, G., 2022. Development of stimulus-sensitive electrospun membranes based on novel biodegradable segmented polyurethane as triggered delivery system for doxorubicin. Biomater. Adv. 136. https://doi.org/10.1016/j.bioadv.2022.212769.

Fisher, M.F., Rao, S.S., 2020. Three-dimensional culture models to study drug resistance in breast cancer. Biotechnol. Bioeng. 117, 2262–2278. https://doi.org/10.1002/bit.27356.

Fontoura, J.C., Viezzer, C., dos Santos, F.G., Ligabue, R.A., Weinlich, R., Puga, R.D., Antonow, D., Severino, P., Bonorino, C., 2020. Comparison of 2D and 3D cell culture models for cell growth, gene expression and drug resistance. Mater. Sci. Eng. C 107, 110264. https://doi.org/10.1016/j.msec.2019.110264.

Gao, N., Xing, C., Wang, H., Feng, L., Zeng, X., Mei, L., Peng, Z., 2019. pH-responsive dual drug-loaded nanocarriers based on poly (2-Ethyl-2-Oxazoline) modified black phosphorus nanosheets for cancer chemo/photothermal therapy. Front. Pharmacol. 10, 450572. https://doi.org/10.3389/fphar.2019.00270.

Giammona, G., Drago, S.E., Calabrese, G., Varvarà, P., Rizzo, M.G., Mauro, N., Nicotra, G., Conoci, S., Pitarresi, G., 2022. Galactosylated polymer/gold nanorods nanocomposites for sustained and pulsed chemo-photothermal treatments of hepatocarcinoma. Pharmaceutics 14, 2503. https://doi.org/10.3390/pharmaceutics14112503.

Gilkes, D.M., Semenza, G.L., Wirtz, D., 2014. Hypoxia and the extracellular matrix: drivers of tumour metastasis. Nat. Rev. Cancer 14, 430–439. https://doi.org/10.1038/nrc3726.

Guo, X., Cheng, Y., Zhao, X., Luo, Y., Chen, J., Yuan, W.E., 2018. Advances in redox-responsive drug delivery systems of tumor microenvironment. J. Nanobiotechnology 16, 74. https://doi.org/10.1186/S12951-018-0398-2.

Hegyi, G., Szigeti, G.P., Szász, A., 2013. Hyperthermia versus oncothermia: Cellular effects in complementary cancer therapy. Evid. Based. Complement. Alternat. Med. https://doi.org/10.1155/2013/672873.

Hendel, T., Wuithschick, M., Kettemann, F., Birnbaum, A., Rademann, K., Polte, J., 2014. In situ determination of colloidal gold concentrations with UV-vis spectroscopy: limitations and perspectives. Anal. Chem. 86, 11115–11124. https://doi.org/10.1021/ac502053s.

Hervault, A., Thanh, N.T.K., 2014. Magnetic nanoparticle-based therapeutic agents for thermo-chemotherapy treatment of cancer. Nanoscale 6, 11553–11573. https://doi.org/10.1039/c4nr03482a.

Hu, J.J., Cheng, Y.J., Zhang, X.Z., 2018. Recent advances in nanomaterials for enhanced photothermal therapy of tumors. Nanoscale 10, 22657–22672. https://doi.org/10.1039/c8nr07627h.

Hu, X., Liu, S., Zhou, G., Huang, Y., Xie, Z., Jing, X., 2014. Electrospinning of polymeric nanofibers for drug delivery applications. J. Control. Release 185, 12–21. https://doi.org/10.1016/j.jconrel.2014.04.018.

Huang, C., Dong, J., Zhang, Y., Chai, S., Wang, X., Kang, S., Yu, D., Wang, P., Jiang, Q., 2021. Gold nanoparticles-loaded polyvinylpyrrolidone/ethylcellulose coaxial electrospun nanofibers with enhanced osteogenic capability for bone tissue regeneration. Mater. Des. 212, 110240. https://doi.org/10.1016/j.matdes.2021.110240.

Huang, X., El-Sayed, I.H., Qian, W., El-Sayed, M.A., 2006. Cancer cell imaging and photothermal therapy in the near-infrared region by using gold nanorods. J. Am. Chem. Soc. 128, 2115–2120. https://doi.org/10.1021/ja057254a.

Javanmardi, S., Tamaddon, A.M., Aghamaali, M.R., Ghahramani, L., Abolmaali, S.S., 2020. Redox-sensitive, PEG-shielded carboxymethyl PEI nanogels silencing MicroRNA-21, sensitizes resistant ovarian cancer cells to cisplatin. Asian J. Pharm. Sci. 15, 69–82. https://doi.org/10.1016/j.ajps.2018.10.006.

Jin, H.O., An, S., Lee, H.C., Woo, S.H., Seo, S.K., Choe, T.B., Yoo, D.H., Lee, S.B., Um, H. D., Lee, S.J., Park, M.J., Kim, J.I., Hong, S.I., Rhee, C.H., Park, I.C., 2007. Hypoxic condition- and high cell density-induced expression of Redd1 is regulated by activation of hypoxia-inducible factor-1α and Sp1 through the phosphatidylinositol 3-kinase/Akt signaling pathway. Cell. Signal. 19, 1393–1403. https://doi.org/10.1016/j.cellsig.2006.12.014.

Kaplan, J.A., Liu, R., Freedman, J.D., Padera, R., Schwartz, J., Colson, Y.L., Grinstaff, M. W., 2016. Prevention of lung cancer recurrence using cisplatin-loaded superhydrophobic nanofiber meshes. Biomaterials 76, 273–281. https://doi.org/10.1016/j.biomaterials.2015.10.060.

Karlsson, H., Fryknäs, M., Larsson, R., Nygren, P., 2012. Loss of cancer drug activity in colon cancer HCT-116 cells during spheroid formation in a new 3-D spheroid cell culture system. Exp. Cell Res. 318, 1577–1585. https://doi.org/10.1016/j.yexcr.2012.03.026.

Karthikeyan, L., Vivek, R., 2022. Synergistic anti-cancer effects of NIR-light responsive nanotherapeutics for chemo-photothermal therapy and photothermal immunotherapy: A combined therapeutic approach. Adv. Cancer Biol. - Metastasis 4, 100044. https://doi.org/10.1016/j.adcanc.2022.100044.

Khan, M.I., Hossain, M.I., Hossain, M.K., Rubel, M.H.K., Hossain, K.M., Mahfuz, A.M.U. B., Anik, M.I., 2022. Recent progress in nanostructured smart drug delivery systems for cancer therapy: A review. ACS Appl. Bio Mater. 5, 971–1012. https://doi.org/10.1021/acsabm.2c00002.

Khodadadi, M., Alijani, S., Montazeri, M., Esmaeilizadeh, N., Sadeghi-Soureh, S., Pilehvar-Soltanahmadi, Y., 2020. Recent advances in electrospun nanofiber-mediated drug delivery strategies for localized cancer chemotherapy. J. Biomed. Mater. Res. Part A 108, 1444–1458. https://doi.org/10.1002/jbm.a.36912.

Kim, J., Singh, B., Shukla, N., Lee, J., Kim, K., Park, M.H., 2022. On-demand drug-delivery platform using electrospun nanofibers by externally triggered glass transition switch. ACS Mater. Lett. 4, 2252–2260. https://doi.org/10.1021/acsmaterialslett.2c00610.

Krause, S., Maffini, M.V., Soto, A.M., Sonnenschein, C., 2010. The microenvironment determines the breast cancer cells' phenotype: Organization of MCF7 cells in 3D cultures. BMC Cancer 10, 263. https://doi.org/10.1186/1471-2407-10-263.

Kuang, G., Lin, X., Li, J., Sun, W., Zhang, Q., Zhao, Y., 2024. Electrospun nanofibers-derived functional scaffolds for cancer therapy. Chem. Eng. J. 489, 151253. https://doi.org/10.1016/j.cej.2024.151253.

Lee, M.H., Yang, Z., Lim, C.W., Lee, Y.H., Dongbang, S., Kang, C., Kim, J.S., 2013. Disulfide-cleavage-triggered chemosensors and their biological applications. Chem. Rev. 113, 5071–5109. https://doi.org/10.1021/cr300358b.

Li Volsi, A., Scialabba, C., Vetri, V., Cavallaro, G., Licciardi, M., Giammona, G., 2017. Near-Infrared light responsive folate targeted gold nanorods for combined photothermal-chemotherapy of osteosarcoma. ACS Appl. Mater. Interfaces 9. https://doi.org/10.1021/acsami.7b03711.

Licciardi, M., Varvarà, P., Tranchina, L., Puleio, R., Cicero, L., Cassata, G., Giammona, G., 2022. In vivo efficacy of verteporfin loaded gold nanorods for combined photothermal/photodynamic colon cancer therapy. Int. J. Pharm. 625. https://doi.org/10.1016/j.ijpharm.2022.122134.

Liebmann, J.E., Cook, J.A., Lipschultz, C., Teague, D., Fisher, J., Mitchell, J.B., 1993. Cytotoxic studies of paclitaxel (Taxol) in human tumour cell lines. Br. J. Cancer 68, 1104–1109. https://doi.org/10.1038/bjc.1993.488.

Link, S., Mohamed, M.B., El-Sayed, M.A., 1999. Simulation of the optical absorption spectra of gold nanorods as a function of their aspect ratio and the effect of the medium dielectric constant. J. Phys. Chem. B. https://doi.org/10.1021/jp990183f.

Liu, P., 2019. Redox- and pH-responsive polymeric nanocarriers. Stimuli responsive polym. nanocarriers drug deliv. Appl. Adv. Nanocarriers Ther. 2, 3–36. https://doi.org/10.1016/b978-0-08-101995-5.00001-5.

Liu, H., Fu, Y., Li, Y., Ren, Z., Li, X., Han, G., Mao, C., 2016. A Fibrous Localized drug delivery platform with NIR-triggered and optically monitored drug release. Langmuir 32, 9083–9090. https://doi.org/10.1021/acs.langmuir.6b02227.

Liu, S., Zhou, G., Liu, D., Xie, Z., Huang, Y., Wang, X., Wu, W., Jing, X., 2012. Inhibition of orthotopic secondary hepatic carcinoma in mice by doxorubicin-loaded electrospun polylactide nanofibers. J. Mater. Chem. B 1, 101–109. https://doi.org/10.1039/c2tb00121g.

Lobato, F.S., Libotte, G.B., Platt, G.M., 2023. Optimization of hyperthermia process applied to cancer treatment using multi-objective optimization differential evolution. J. Therm. Biol. 111, 103400. https://doi.org/10.1016/j.jtherbio.2022.103400.

Luo, Y., Wei, X., Wan, Y., Lin, X., Wang, Z., Huang, P., 2019. 3D printing of hydrogel scaffolds for future application in photothermal therapy of breast cancer and tissue repair. Acta Biomater. 92, 37–47. https://doi.org/10.1016/j.actbio.2019.05.039.

Lv, D., Hu, Z., Lu, L., Lu, H., Xu, X., 2017. Three-dimensional cell culture: A powerful tool in tumor research and drug discovery. Oncol. Lett. 14, 6999. https://doi.org/10.3892/ol.2017.7134.

Ma, P., Mumper, R.J., 2013. Paclitaxel Nano-Delivery Systems: A Comprehensive Review. J. Nanomed. Nanotechnol. 4, 1000164. https://doi.org/10.4172/2157-7439.1000164.

Ma, Y., Wang, X., Zong, S., Zhang, Z., Xie, Z., Huang, Y., Yue, Y., Liu, S., Jing, X., 2015. Local, combination chemotherapy in prevention of cervical cancer recurrence after surgery by using nanofibers co-loaded with cisplatin and curcumin. RSC Adv. 5, 106325–106332. https://doi.org/10.1039/c5ra17230f.

Ma, W., Wang, X., Zhang, D., Mu, X., 2024. Research progress of disulfide bond based tumor microenvironment targeted drug delivery system. Int. J. Nanomedicine 19, 7547–7566. https://doi.org/10.2147/ijn.s471734.

Mahmoud, N.N., Qabooq, H., Alsotari, S., Tarawneh, O.A., Aboalhaija, N.H., Shraim, S., Alkilany, A.M., Khalil, E.A., Abu-Dahab, R., 2021. Quercetin-gold nanorods incorporated into nanofibers: development, optimization and cytotoxicity. RSC Adv. 11, 19956–19966. https://doi.org/10.1039/d1ra02004h.

Martorana, A., Fiorica, C., Palumbo, F.S., Federico, S., Giammona, G., Pitarresi, G., 2023. Redox responsive 3D-printed nanocomposite polyurethane-urea scaffold for Doxorubicin local delivery. J. Drug Deliv. Sci. Technol. 88, 104890. https://doi.org/10.1016/j.jddst.2023.104890.

Mazidi, Z., Javanmardi, S., Naghib, S.M., Mohammadpour, Z., 2022. Smart stimuli-responsive implantable drug delivery systems for programmed and on-demand cancer treatment: An overview on the emerging materials. Chem. Eng. J. 433, 134569. https://doi.org/10.1016/j.cej.2022.134569.

Melamed, J.R., Edelstein, R.S., Day, E.S., 2015. Elucidating the fundamental mechanisms of cell death triggered by photothermal therapy. ACS Nano 9, 6–11. https://doi.org/10.1021/acsnano.5b00021.

Nogueira, P.F.M., Marangoni, V.S., Zucolotto, V., 2020. The aspect ratio of gold nanorods as a cytotoxicity factor on Raphidocelis subcaptata. Environ. Res. 191. https://doi.org/10.1016/j.envres.2020.110133.

Overchuk, M., Weersink, R.A., Wilson, B.C., Zheng, G., 2023. Photodynamic and Photothermal Therapies: Synergy Opportunities for Nanomedicine. ACS Nano 17, 7979–8003. https://doi.org/10.1021/acsnano.3c00891.

Padmakumar, S., Amiji, M.M., 2023. Long-acting therapeutic delivery systems for the treatment of gliomas. Adv. Drug Deliv. Rev. 197, 114853. https://doi.org/10.1016/j.addr.2023.114853.

Palumbo, F.S., Federico, S., Pitarresi, G., Fiorica, C., Giammona, G., 2021. Synthesis and characterization of redox-sensitive polyurethanes based on L-glutathione oxidized and poly(ether ester) triblock copolymers. React. Funct. Polym. 166. https://doi.org/10.1016/j.reactfunctpolym.2021.104986.

Pamplona, R., González-Lana, S., Ochoa, I., Martín-Rapún, R., Sánchez-Somolinos, C., 2024. Evaluation of gelatin-based hydrogels for colon and pancreas studies using 3D in vitro cell culture. J. Mater. Chem. B 12, 3144–3160. https://doi.org/10.1039/d3tb02640j.

Panthi, V.K., Bashyal, S., Paudel, K.R., 2024. Docetaxel-loaded nanoformulations delivery for breast cancer management: Challenges, recent advances, and future perspectives. J. Drug Deliv. Sci. Technol. 92, 105314. https://doi.org/10.1016/j.jddst.2023.105314.

Petersen, O.W., Rønnov-Jessen, L., Howlett, A.R., Bissell, M.J., 1992. Interaction with basement membrane serves to rapidly distinguish growth and differentiation pattern of normal and malignant human breast epithelial cells. Proc. Natl. Acad. Sci. 89, 9064–9068. https://doi.org/10.1073/pnas.89.19.9064.

Poláková, L., Širc, J., Hobzová, R., Cocârță, A.I., Heřmánková, E., 2019. Electrospun nanofibers for local anticancer therapy: Review of in vivo activity. Int. J. Pharm. 558, 268–283. https://doi.org/10.1016/j.ijpharm.2018.12.059.

Qian, Q., Song, J., Chen, C., Pu, Q., Liu, X., Wang, H., 2023. Recent advances in hydrogels for preventing tumor recurrence. Biomater. Sci. 11, 2678–2692. https://doi.org/10.1039/d3bm00003f.

Qiu, Y., Liu, Y., Wang, L., Xu, L., Bai, R., Ji, Y., Wu, X., Zhao, Y., Li, Y., Chen, C., 2010. Surface chemistry and aspect ratio mediated cellular uptake of Au nanorods. Biomaterials 31, 7606–7619. https://doi.org/10.1016/j.biomaterials.2010.06.051.

Qu, Y., Chu, B.Y., Peng, J.R., Liao, J.F., Qi, T.T., Shi, K., Zhang, X.N., Wei, Y.Q., Qian, Z. Y., 2015. A biodegradable thermo-responsive hybrid hydrogel: therapeutic applications in preventing the post-operative recurrence of breast cancer. NPG Asia Mater. 7, e207.

Quinn, J.F., Whittaker, M.R., Davis, T.P., 2016. Glutathione responsive polymers and their application in drug delivery systems. Polym. Chem. 8, 97–126. https://doi.org/10.1039/c6py01365a.

Ramachandran, R., Junnuthula, V.R., Gowd, G.S., Ashokan, A., Thomas, J., Peethambaran, R., Thomas, A., Unni, A.K.K., Panikar, D., Nair, S.V., Koyakutty, M., 2017. Theranostic 3-Dimensional nano brain-implant for prolonged and localized treatment of recurrent glioma. Sci. Reports 7, 43271. https://doi.org/10.1038/srep43271.

Ren, F., Bhana, S., Norman, D.D., Johnson, J., Xu, L., Baker, D.L., Parrill, A.L., Huang, X., 2013. Gold nanorods carrying paclitaxel for photothermal-chemotherapy of cancer. Bioconjug. Chem. 24, 376–386. https://doi.org/10.1021/bc300442d.

Ribeiro, T.P., Moreira, J.A., Monterio, F.J., Laranjeira, M.S., 2022. Nanomaterials in cancer: Reviewing the combination of hyperthermia and triggered chemotherapy. J. Control. Release 347, 89–103. https://doi.org/10.1016/j.jconrel.2022.04.045.

Roskov, K.E., Kozek, K.A., Wu, W.C., Chhetri, R.K., Oldenburg, A.L., Spontak, R.J., Tracy, J.B., 2011. Long-range alignment of gold nanorods in electrospun polymer nano/microfibers. Langmuir 27, 13965–13969. https://doi.org/10.1021/la2021066.

Roti, J.L., 2008. Cellular responses to hyperthermia (40–46°C): Cell killing and molecular events. Int. J. Hyperth. 24, 3–15. https://doi.org/10.1080/02656730701769841.

Rybak, D., Su, Y.C., Li, Y., Ding, B., Lv, X., Li, Z., Yeh, Y.C., Nakielski, P., Rinoldi, C., Pierini, F., Dodda, J.M., 2023. Evolution of nanostructured skin patches towards multifunctional wearable platforms for biomedical applications. Nanoscale 15, 8044–8083. https://doi.org/10.1039/d3nr00807j.

Salehi, S.S., Mirmiranpour, H., Rabizadeh, S., Esteghamati, A., Tomasello, G., Alibakhshi, A., Najafi, N., Rajab, A., Nakhjavani, M., 2021. Improvement in redox homeostasis after cytoreductive surgery in colorectal adenocarcinoma. Oxid. Med. Cell. Longev. 8864905. https://doi.org/10.1155/2021/8864905.

Sang, S., Jiang, Z., Xie, N., Rao, H., Liao, K., Hu, Q., Zhang, Z., Guo, R., Fan, T., Deng, K., 2021. Black phosphorus nanosheets and paclitaxel encapsulated hydrogel for synergistic photothermal-chemotherapy. Nanophotonics 10, 2625–2637. https://doi.org/10.1515/nanoph-2021-0089.

Scarabelli, L., Sánchez-Iglesias, A., Pérez-Juste, J., Liz-Marzán, L.M., 2015. A "Tips and Tricks" practical guide to the synthesis of gold nanorods. J. Phys. Chem. Lett. 6. https://doi.org/10.1021/acs.jpclett.5b02123.

Shaha, S., Rodrigues, D., Mitragotri, S., 2024. Locoregional drug delivery for cancer therapy: Preclinical progress and clinical translation. J. Control. Release 367, 737–767. https://doi.org/10.1016/j.jconrel.2024.01.072.

Sharifi-Rad, J., Quispe, C., Patra, J.K., Singh, Y.D., Panda, M.K., Das, G., Adetunji, C.O., Michael, O.S., Sytar, O., Polito, L., Živković, J., Cruz-Martins, N., Klimek-Szczykutowicz, M., Ekiert, H., Choudhary, M.I., Ayatollahi, S.A., Tynybekov, B., Kobarfard, F., Muntean, A.C., Grozea, I., Daştan, S.D., Butnariu, M., Szopa, A., Calina, D., 2021. Paclitaxel: Application in modern oncology and nanomedicine-based cancer therapy. Oxid. Med. Cell. Longev. 2021. https://doi.org/10.1155/2021/3687700.

Sheta, E.A., Trout, H., Gildea, J.J., Harding, M.A., Theodorescu, D., 2001. Cell density mediated pericellular hypoxia leads to induction of HIF-1alpha via nitric oxide and Ras/MAP kinase mediated signaling pathways. Oncogene 20, 7624–7634. https://doi.org/10.1038/sj.onc.1204972.

Singh, B., Kim, J., Shukla, N., Lee, J., Kim, K., Park, M.H., 2023. Smart delivery platform using core-shell nanofibers for sequential drug release in wound healing. ACS Appl. Bio Mater. 6, 2314–2324. https://doi.org/10.1021/acsabm.3c00178.

Su, Y., Liu, Y., Xu, X., Zhou, J., Xu, L., Xu, X., Wang, D., Li, M., Chen, K., Wang, W., 2018. On-Demand versatile prodrug nanomicelle for tumor-specific bioimaging and photothermal-chemo synergistic cancer therapy. ACS Appl. Mater. Interfaces 10, 38700–38714. https://doi.org/10.1021/acsami.8b11349.

Sun, B., Luo, C., Yu, H., Zhang, X., Chen, Q., Yang, W., Wang, M., Kan, Q., Zhang, H., Wang, Y., He, Z., Sun, J., 2018. Disulfide bond-driven oxidation- and reduction-responsive prodrug nanoassemblies for cancer therapy. Nano Lett. 18, 3643–3650. https://doi.org/10.1021/acs.nanolett.8b00737.

Taddei, M.L., Giannoni, E., Comito, G., Chiarugi, P., 2013. Microenvironment and tumor cell plasticity: An easy way out. Cancer Lett. 341, 80–96. https://doi.org/10.1016/j.canlet.2013.01.042.

Talebian, S., Foroughi, J., Wade, S.J., Vine, K.L., Dolatshahi-Pirouz, A., Mehrali, M., Conde, J., Wallace, G.G., 2018. Biopolymers for antitumor implantable drug delivery systems: recent advances and future outlook. Adv. Mater. 30, 1706665. https://doi.org/10.1002/adma.201706665.

Tayebi-Khorrami, V., Rahmanian-Devin, P., Fadaei, M.R., Movaffagh, J., Askari, V.R., 2024. Advanced applications of smart electrospun nanofibers in cancer therapy: With insight into material capabilities and electrospinning parameters. Int. J. Pharm. X 8, 100265. https://doi.org/10.1016/j.ijpx.2024.100265.

Thannhauser, T.W., Konishi, Y., Scheraga, H.A., 1987. Analysis for disulfide bonds in peptides and proteins. Methods Enzymol. 143, 115–119. https://doi.org/10.1016/0076-6879(87)43020-6.

Tian, Yu., Tian, R., Chen, L.i., Jin, R., Feng, Y., Bai, Y., Chen, X., Tian, Y., Tian, R., Chen, L., Jin, R., Feng, Y., Bai, Y., Chen, X., 2019. Redox-responsive nanogel with intracellular reconstruction and programmable drug release for targeted tumor therapy. Macromol. Rapid Commun. 40, 1800824. https://doi.org/10.1002/marc.201800824.

Tiwari, A.P., Hwang, T.I., Oh, J.M., Maharjan, B., Chun, S., Kim, B.S., Joshi, M.K., Park, C.H., Kim, C.S., 2018. PH/NIR-Responsive polypyrrole-functionalized fibrous localized drug-delivery platform for synergistic cancer therapy. ACS Appl. Mater. Interfaces 10, 20256–20270. https://doi.org/10.1021/acsami.7b17664.

Tran, T.H., Nguyen, H.T., Pham, T.T., Choi, J.Y., Choi, H.G., Yong, C.S., Kim, J.O., 2015. Development of a graphene oxide nanocarrier for dual-drug chemo-phototherapy to overcome drug resistance in cancer. ACS Appl. Mater. Interfaces 7, 28647–28655. https://doi.org/10.1021/acsami.5b10426.

Turner, J.G., Og, J.H., Murphy, C.J., 2020. Gold nanorod impact on mechanical properties of stretchable hydrogels. Soft Matter 16, 6582–6590. https://doi.org/10.1039/d0sm00737d.

Varvarà, P., Tranchina, L., Cavallaro, G., Licciardi, M., 2020. Preparation and characterization of gold nanorods coated with gellan gum and lipoic acid. Appl. Sci. 10. https://doi.org/10.3390/app10238322.

Wang, X., Wang, C., Wang, X., Wang, Y., Zhang, Q., Cheng, Y., 2017. A polydopamine nanoparticle-knotted poly(ethylene glycol) hydrogel for on-demand drug delivery and chemo-photothermal therapy. Chem. Mater. 29, 1370–1376. https://doi.org/10.1021/acs.chemmater.6b05192.

Wang, X., Li, C., Wang, Y., Chen, H., Zhang, X., Luo, C., Zhou, W., Li, L., Teng, L., Yu, H., Wang, J., 2022. Smart drug delivery systems for precise cancer therapy. Acta Pharm. Sin. B 12, 4098. https://doi.org/10.1016/j.apsb.2022.08.013.

Wei, X., Liu, C., Wang, Z., Luo, Y., 2020. 3D printed core-shell hydrogel fiber scaffolds with NIR-triggered drug release for localized therapy of breast cancer. Int. J. Pharm. 580, 119219. https://doi.org/10.1016/j.ijpharm.2020.119219.

Wells, C.M., Harris, M., Choi, L., Murali, V.P., Guerra, F.D., Jennings, J.A., 2019. Stimuli-responsive drug release from smart polymers. J. Funct. Biomater. 10. https://doi.org/10.3390/jfb10030034.

Wolinsky, J.B., Colson, Y.L., Grinstaff, M.W., 2012. Local drug delivery strategies for cancer treatment: Gels, nanoparticles, polymeric films, rods, and wafers. J. Control. Release 159, 14–26. https://doi.org/10.1016/j.jconrel.2011.11.031.

Woodring, R.N., Gurysh, E.G., Bachelder, E.M., Ainslie, K.M., 2023. Drug delivery systems for localized cancer combination therapy. ACS Appl. Bio Mater. 6, 934–950. https://doi.org/10.1021/acsabm.2c00973.

Xiao, R., Zhou, G., Wen, Y., Ye, J., Li, X., Wang, X., 2023. Recent advances on stimuli-responsive biopolymer-based nanocomposites for drug delivery. Compos. Part B Eng. 266, 111018. https://doi.org/10.1016/j.compositesb.2023.111018.

Xu, N., Zhang, X., Qi, T., Wu, Y., Xie, X., Chen, F., Shao, D., Liao, J., 2022. Biomedical applications and prospects of temperature-orchestrated photothermal therapy. MedComm – Biomater. Appl. 1, e25.

Yang, G., Wang, J., Wang, Y., Li, L., Guo, X., Zhou, S., 2015. An implantable active-targeting micelle-in-nanofiber device for efficient and safe cancer therapy. ACS Nano 9, 1161–1174. https://doi.org/10.1021/nn504573u.

Yeung, T.M., Gandhi, S.C., Wilding, J.L., Muschel, R., Bodmer, W.F., 2010. Cancer stem cells from colorectal cancer-derived cell lines. Proc. Natl. Acad. Sci. U. S. A. 107, 3722. https://doi.org/10.1073/pnas.0915135107.

You, J., Shao, R., Wei, X., Gupta, S., Li, C., 2010. Near-infrared light triggers release of paclitaxel from biodegradable microspheres: Photothermal effect and enhanced antitumor activity. Small 6, 1022–1031. https://doi.org/10.1002/smll.201000028.

Yu, Q., Han, Y., Tian, T., Zhou, Q., Yi, Z., Chang, J., Wu, C., 2019. Chinese sesame stick-inspired nano-fibrous scaffolds for tumor therapy and skin tissue reconstruction. Biomaterials 194, 25–35. https://doi.org/10.1016/j.biomaterials.2018.12.012.

Zeng, Y., Ma, J., Zhan, Y., Xu, X., Zeng, Q., Liang, J., Chen, X., 2018. Hypoxia-activated prodrugs and redox-responsive nanocarriers. Int. J. Nanomedicine 13, 6551–6574. https://doi.org/10.2147/ijn.s173431.

Zhang, M., Hu, W., Cai, C., Wu, Y., Li, J., Dong, S., 2022. Advanced application of stimuli-responsive drug delivery system for inflammatory arthritis treatment. Mater. Today Bio 14, 100223. https://doi.org/10.1016/j.mtbio.2022.100223.

Zhang, Y., Jiang, C., 2021. Postoperative cancer treatments: In-situ delivery system designed on demand. J. Control. Release 330, 554–564. https://doi.org/10.1016/j.jconrel.2020.12.038.

Zhang, L., Liao, W., Chen, S., Chen, Y., Cheng, P., Lu, X., Ma, Y., 2023a. Towards a New 3Rs Era in the construction of 3D cell culture models simulating tumor microenvironment. Front. Oncol. 13. https://doi.org/10.3389/fonc.2023.1146477.

Zhang, Y., Liu, S., Wang, X., Zhang, Z.Y., Jing, X.B., Zhang, P., Xie, Z.G., 2014. Prevention of local liver cancer recurrence after surgery using multilayered cisplatin-loaded polylactide electrospun nanofibers. Chinese J. Polym. Sci. 32, 1111–1118. https://doi.org/10.1007/S10118-014-1491-0.

Zhang, X., Wei, H., Dong, C., Wang, J., Zhang, T., Huang, L., Ni, D., Luo, Y., 2023b. 3D printed hydrogel/bioceramics core/shell scaffold with NIR-II triggered drug release for chemo-photothermal therapy of bone tumors and enhanced bone repair. Chem. Eng. J. 461, 141855. https://doi.org/10.1016/j.cej.2023.141855.

Zhao, J., Cui, W., 2020. Functional electrospun fibers for local therapy of cancer. Adv. Fiber Mater. 2, 229–245. https://doi.org/10.1007/S42765-020-00053-9.

Zhao, Y., Yao, R., Ouyang, L., Ding, H., Zhang, T., Zhang, K., Cheng, S., Sun, W., 2014. Three-dimensional printing of Hela cells for cervical tumor model in vitro. Biofabrication 6, 035001. https://doi.org/10.1088/1758-5082/6/3/035001.

Zhao, Y., Peng, X., Xu, X., Wu, M., Sun, F., Xin, Q., Zhang, H., Zuo, L., Cao, Y., Xia, Y., Luo, J., Ding, C., Li, J., 2023. Chitosan based photothermal scaffold fighting against bone tumor-related complications: Recurrence, infection, and defects. Carbohydr. Polym. 300, 120264. https://doi.org/10.1016/j.carbpol.2022.120264.

Zhou, M., Han, S., Aras, O., An, F., 2021. Recent advances in paclitaxel-based self-delivery nanomedicines for cancer therapy. Curr. Med. Chem. 28, 6358. https://doi.org/10.2174/0929867327666201111143725.

Zou, L., Wang, H., He, B., Zeng, L., Tan, T., Cao, H., He, X., Zhang, Z., Guo, S., Li, Y., 2016. Current approaches of photothermal therapy in treating cancer metastasis with nanotherapeutics. Theranostics 6, 762. https://doi.org/10.7150/thno.14988.